INVITED PAPER

Direct Liquid Cooling of High Flux Micro and Nano Electronic Components

Boiling, evaporation, jet, and spray cooling, by suitable liquids such as fluorocarbons, might serve to control chip hot-spots and overheating.

By Avram Bar-Cohen, *Fellow IEEE*, Mehmet Arik, *Member IEEE*, and Michael Ohadi

ABSTRACT | The inexorable rise in chip power dissipation and emergence of on-chip hot spots with heat fluxes approaching 1 kW/cm^2 has turned renewed attention to direct cooling with dielectric liquids. Use of dielectric liquids in intimate contact with the heat dissipating surfaces eliminates the deleterious effects of solid–solid interface resistances and harnesses the highly efficient phase-change processes to the critical thermal management of advanced IC chips. In the interest of defining the state-of-the-art in direct liquid cooling, this paper begins with a discussion of the thermophysics of phase-change processes and a description of the available dielectric liquid cooling techniques and their history. It then describes the phenomenology of pool boiling, spray/jet impingement, gas-assisted evaporation, and synthetic jet impingement with dielectric liquids. Available correlations for predicting the heat transfer coefficients and limiting heat transfer rates, as well as documented empirical results for these promising techniques for on-chip hot spot cooling, are also provided and compared.

KEYWORDS | Dielectric liquids; evaporation; hot spots; immersion cooling; jet impingement; liquid cooling; pool boiling; spray cooling; synthetic jets

NOMENCLATURE

A	Surface area (m^2)
a	Exponent in (1)
C_p	Specific heat (J/kg-K)
COP	Coefficient of performance
D	Drop diameter (m)
d_h	Hydraulic diameter (m)
E	Electric field (V/m)
g	Gravitational acceleration (m/s^2)
G	Mass flux (kg/m^2 − s)
h	Local heat transfer coefficient (W/m^2 − k)
$\overline{h}$	Average heat transfer coefficient (W/m^2 − k)
h_{fg}	Latent heat of vaporization (J/kg)
k	Thermal conductivity (W/m-K)
L	Length (m)
$\dot{m}_{evp}$	Evaporative mass flux (kg/m^2 − s)
m	Exponent in Eq. (18)
n	Exponent in Eq. (18)
Nu	Nusselt number
P	Pressure (Pa)
Pr	Prandtl number
Q	Heat transfer per drop impinging on hot surface (W)
q	Heat flux (W/m^2)
$\overline{r}$	Universal gas constant (8.3145 J/mol-K)
Re	Reynold number
Rg	Gas constant (J/kg-K)
S	Heater surface property
s_{NP}	Nozzle-to-plate distance (m)
t	Thickness of hot plate (m)
T	Temperature (K)
TME	
u, U	Velocity (m/s)
V	Liquid molar volume (m^3/mol)
$\dot{v}$	Local volumetric flux (m/s)
We	Weber number
x, r	Space coordinates (m)

Greek symbols

α	Relative nozzle area
Γ	Mass flow rate per unit width (kg/m-s)

Manuscript received March 27, 2006; revised May 15, 2006.
A. Bar-Cohen and **M. Ohadi** are with the Department of Mechanical Engineering, University of Maryland, College Park, MD 20742 USA (e-mail: abc@umd.edu).
M. Arik is with the Thermal Systems Laboratory, GE Global Research Center, Niskayuna, NY 12309 USA (e-mail:arik@crd.ge.com).
Digital Object Identifier: 10.1109/JPROC.2006.879791

δ	Film thickness (m)
ε	Dielectric permittivity (F/m)
μ	Dynamic viscosity (Ns/m^2)
ν	Kinematic viscosity (m^2/s)
ρ	Density (kg/m^3)
Π	Disjoining pressure (Pa)
σ	Surface tension (N/m)

Subscripts

0	Stagnation point or initial point
a	Ambient fluid
b	Bubble
cr	Critical point
CHF	Critical heat flux
d	Droplet
f	Fluid or film
i	Liquid–vapor interface
J	Jet
l	Liquid
max	Maximum value
S	Slip boundary condition
sat	Saturated state
sub	Subcooled state
SMD	Sauter mean diameter
tr	Transition to turbulent
v	Vapor
w	Wall

I. INTRODUCTION

The Moore's law progression in semiconductor technology, including shrinking feature size, increasing transistor density, and faster circuit speeds, is leading to ever higher chip power dissipations and heat fluxes. Roadmap projections for the high-performance chip category suggest that the maximum chip power dissipation will exceed 300 W and the average chip heat flux exceed 150 W/cm^2 within the next few years [1]. Moreover, in recent years, increasing performance demands have resulted in greater nonuniformity of on-chip power dissipation [2], creating localized submillimeter hotspots with heat fluxes approaching 1 kW/cm^2, whose elevated temperature can degrade the processor performance and reliability. Consequently, new and novel cooling techniques, with the ability to selectively cool submillimeter, high heat flux zones while maintaining chip temperatures below 100 °C with spatial and temporal temperature variations below 10 °C, are needed.

It is unlikely that conventional air and liquid cooling techniques, relying on heat sinks or cold plates, could be extended to deal with the localized high flux zones without severely compromising their overall cooling capability. In particular, the conventional use of thermal interface materials (TIMs) to bridge the silicon chip and the thermal spreader and/or the heat sink/coldplate, introduces a relatively high local thermal resistance, which is incompatible with the effective removal of local heat flux spikes. Thus, the application of conventional thermal packaging technology, developed to provide uniform chip cooling, to such chip designs could be expected to result in lower allowable chip power dissipation or unnecessary overcooling of large areas of the chip.

Alternatively, direct liquid cooling techniques, which eliminate the thermal interface materials and allow for direct contact between a dielectric liquid and the surface of the chip, hold great promise for hot spot-driven thermal management of ICs. Moreover, use of phase-change processes, including pool boiling, gas-assisted evaporative cooling, jet impingement, and spray cooling, exploit the latent heat of these liquids to reduce the required mass flow rates and can provide the added advantage of inherently high heat transfer coefficients. This paper will define, quantify, and then compare these various direct liquid-cooling techniques.

II. THERMODYNAMICS AND HEAT TRANSFER OF EVAPORATION AND BOILING

Evaporation: When liquid in a constant-pressure vessel is uniformly heated at a slow rate, the resulting changes in temperature and volume are related in a characteristic way, as shown in the volume-temperature graph displayed in Fig. 1. Starting at point A, the addition of heat results in a temperature rise and a modest increase in volume until point 1 is reached. Along this all-liquid locus, the amount of heat required to raise the temperature of a unit mass by

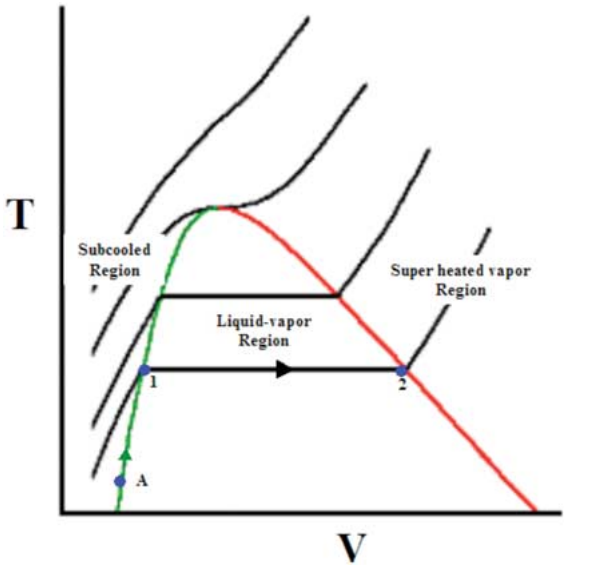

Fig. 1. *Characteristic volume–temperature curves for phase change processes.*

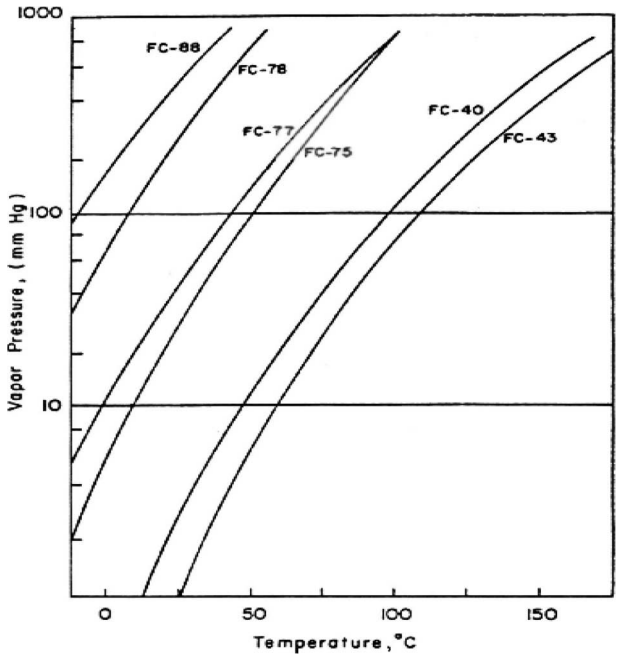

Fig. 2. *Saturation curves for several fluorocarbons [3].*

1° is nearly constant and is referred to as the liquid constant-pressure specific heat C_p. In the region between points 1 and 2, vapor and liquid are present as coexisting phases in equilibrium. The addition of heat increases the vapor fraction, and hence the volume, without altering the temperature of the two-phase mixture. The amount of heat required to convert a unit mass of liquid into vapor is termed the latent heat of vaporization h_{fg}. At point 2 all the liquid has vaporized, and further heating results in a temperature rise of the vapor along a locus appropriate to the vapor constant-pressure specific heat. The termination of the all-liquid state, point 1, and the beginning of the all-vapor state, point 2, are generally referred to as the liquid and vapor saturation points, respectively.

This description pertains to addition of heat to a quantity of liquid at a single constant pressure. If the process is repeated for many different pressures, the "saturation curve" shown in Fig. 2 is obtained. The saturated-liquid line represents the locus of all points 1, and the saturated-vapor line, shown in red, represents the locus of all points 2. It is of interest to note that a "critical" temperature and pressure, at which liquid and vapor molecules are energetically identical and at which no difference exists between the specific volume of the liquid and vapor, can be defined for each fluid. This point corresponds to the top of the dome in Fig. 1.

Because of the higher internal energy of a vapor molecule relative to a liquid molecule of the same species and at the same temperature, evaporation of a fluid, under conditions far removed from the critical point, generally results in the absorption of a very substantial amount of heat. Rapid evaporation thus facilitates the transfer of a very high heat flux from the surface wetted by the fluid. The migration or diffusion of vapor, generated at the free liquid-vapor interface by this evaporation process, is governed by the difference in vapor pressure or vapor concentration between the interface and the ambient. Along the interface, it is generally assumed that the vapor and the liquid are in thermodynamic equilibrium; therefore, the vapor pressure at the interface corresponds to the saturation value at the local liquid temperature. Vapor pressures for several fluorocarbons in the range of relevant temperatures are shown in Fig. 2.

Boiling: Although boiling, like evaporation, involves a change from the liquid to the vapor phase, in contrast to evaporation, boiling generally refers to a process that occurs along solid surfaces submerged in the liquid and is characterized by the dominant influence of vapor bubbles. Boiling typically commences when the surface temperature exceeds the liquid saturation temperature (the boiling point) by 3 °C to 10 °C, and vapor bubbles are then found to grow and issue from minute cavities in the surface [4].

In the analysis and correlation of boiling phenomena, it is convenient to distinguish between pool boiling, referring to boiling in an initially quiescent liquid, and flow boiling, referring to boiling in the presence of a strong velocity field, as may occur, for example, in pipe flow or in jet impingement on a surface. Furthermore, since the boiling process depends primarily on the temperature of the heated surface, both subcooled boiling, during which the bulk liquid is below the saturation temperature, and saturated boiling, during which the bulk temperature is uniformly at the saturation temperature, may be observed.

For a surface experiencing boiling heat transfer, the variation of heat flux results in a characteristic temperature response at the surface, reflecting a progression through particular regimes of ebullient heat transfer. This behavior is generally represented as a log–log plot of the heat flux q versus the surface superheat $T_w - T_{sat}$, giving rise to the so-called Nukiyama boiling curve. A typical "boiling curve" for saturated pool boiling is shown in Fig. 3(a). At low heat flux levels, single-phase natural convection is the dominant heat removal mechanism (section AB on the boiling curve). At sufficiently large wall superheats, typically 3–5 K for water as well as FC liquids under ideal conditions, nucleate boiling begins on the heater surface. The highly efficient nucleate boiling heat transfer mode is characterized by the formation and departure of vapor bubbles at the heated surface. Following incipience, at approximately 2 W/cm^2 for FC liquids under ideal conditions, a further order-of-magnitude increase in the heat flux can be accommodated in nucleate boiling with a modest 10 °C–20 °C increase in the heater temperature (section CD).

In the boiling of the highly wetting dielectric liquids, the onset of nucleate boiling is often accompanied by a

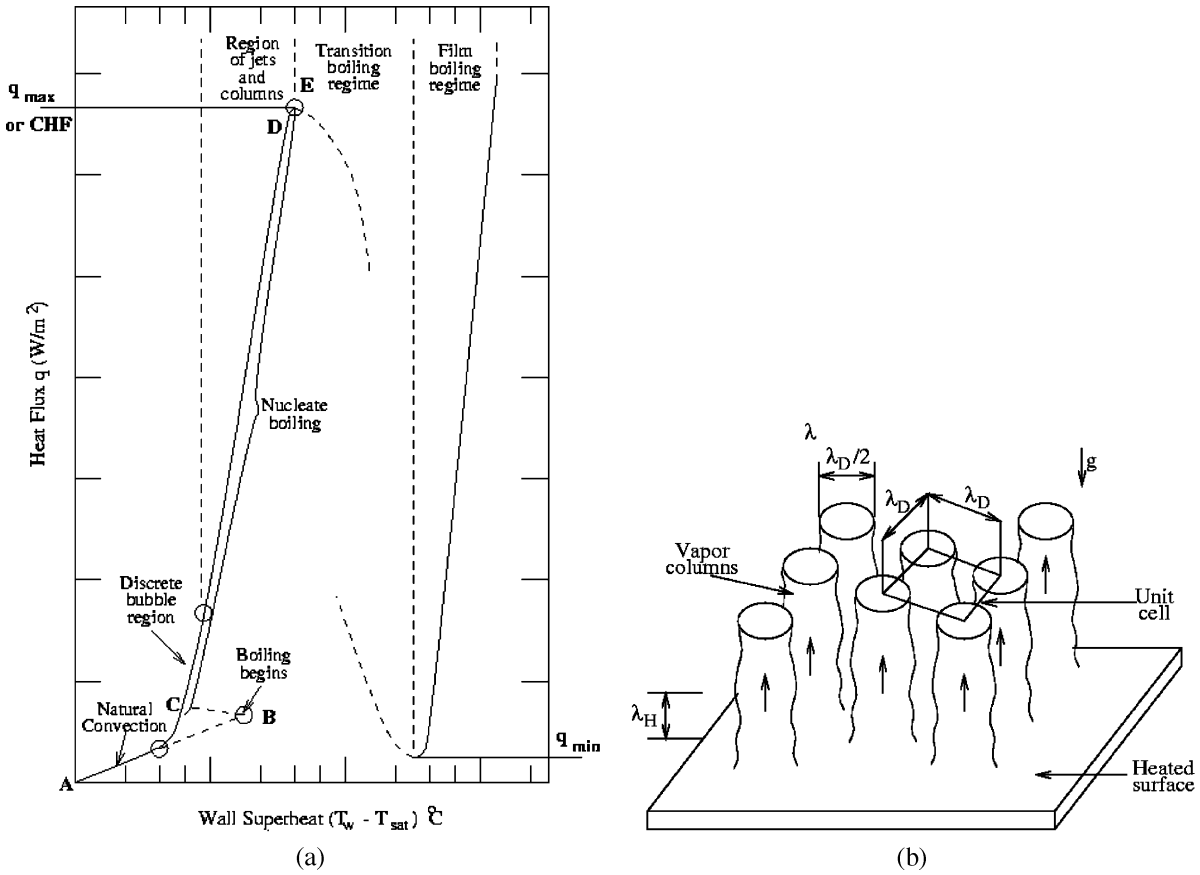

Fig. 3. *(a) Typical pool boiling curve. (b) Vapor column configuration [21].*

large reduction in the heater temperature. The difference in the wall superheats before and after boiling incipience is called the "incipience overshoot." A comprehensive review of this phenomenon has been provided by Bar-Cohen and Simon [5].

In the nucleate boiling regime, the bubbles increase in size with increasing heat flux at the heater surface and begin to coalesce to form larger bubbles. As this process continues, the bubbles become larger and larger until they form a large vapor mushroom, which is attached to the heater surface by adjacent columns of vapor and liquid. The critical heat flux (CHF) (point E) places an upper limit on nucleate boiling heat transfer. At CHF, typically occurring at 15–20 W/cm^2 for saturated FC liquids at atmospheric pressure, the vapor generation rate is so high that the heated surface becomes partially or completely blanketed by vapor and the boiling mechanism changes to film boiling.

In film boiling, the vapor blanket on the heater may periodically thin or even break, thus allowing the liquid to touch the heater surface and temporarily resume nucleation on a small fraction of the heated surface.

Thin-Film Phase Change: Heat transfer through liquid films can occur by a variety of mechanisms. For low thermal conductivity films that are substantially thicker than the bubble departure diameter, boiling will occur along the wetted surface. However, for high conductivity thin films, the superheat at the wall may be insufficient to initiate and sustain nucleate boiling. In such configurations, heat transfer can be expected to occur largely by conduction through the film and evaporation at the liquid–vapor interface. In intermediate configurations, bubbles produced by sporadic boiling along the surfaces wet by such thin liquid films may burst through the liquid film, temporarily enhancing both conductive and evaporative thermal transport from the wall.

III. HISTORY OF DIRECT LIQUID COOLING

While the inherent advantages of liquid coolants have been exploited for nearly 60 years in thermal control of "macro" electronic components like power transistors, traveling wave tubes, klystron tubes, and power supplies, liquid cooling of microelectronic components began to attract serious attention only in the mid-1980s, when indirectly water-cooled mainframe computers were introduced by IBM, Honeywell, Sperry-Univac, Control Data, and

Hitachi. Despite a relatively primitive implementation of liquid cooling, these liquid-cooled computers offered significant improvements in circuit density and heat removal capability relative to previous designs [6]. The initial success of water-cooled computers in the marketplace demonstrated the performance enhancements and "barrier busting" that could be achieved by aggressive cooling and set the stage for the development of more advanced thermal control techniques.

The ever-present solid–solid interfacial resistance limits the thermal efficacy of indirect liquid cooling techniques, which involve conductive heat removal at the chip or chip package followed by convection to a liquid. To overcome this limitation, attention was directed to the enormous promise of direct liquid cooling, both in the form of miniaturized, compact heat exchangers, or microchannels, etched into the silicon chips [7] and immersion of bare chips in dielectric liquids, as well as the impingement of these liquids on the chip surfaces [8], [9]. Four supercomputer designs, including the Cray-2 using immersion in a perflourinated liquid [10], the Cray-3 using gas-assisted evaporation of a perflourinated liquid [11], CDC's ETA-10 using immersion in liquid nitrogen [12], and the Supercomputer Systems Inc. SS-1 using submerged impinging liquid jets [13], employed direct contact of dielectric liquids with the external surface to directly cool high-performance chips.

Thermal control of operational avionic components by direct immersion in low boiling point fluids dates back to open-cycle pool evaporators developed in the late 1940s. When both high heat dissipation rates and long operating periods are encountered, the vapor generated in the immersion cooler must be condensed and recirculated. This can be done with a remote condenser, connected by appropriate piping to the immersion module, by condensing surfaces placed directly in the vapor space above the evaporating/boiling liquid, or by submerging the heat exchanger in the liquid, as described in [4], [15], and [16].

IV. CANDIDATE DIELECTRIC LIQUIDS

The direct cooling of microelectronic components imposes stringent chemical, electrical, and thermal requirements on the liquids to be used in this thermal control mode. Direct liquid cooling of microelectronic components requires compatibility between the liquid coolant and a system-specific combination of the chip, chip package, substrate, and printed circuit board materials, e.g., silicon, silicon dioxide, silicon nitride, alumina, o-rings, plastic encapsulants, solder, gold, and epoxy glass. A liquid coolant must possess the dielectric strength needed to provide electrical isolation between adjacent power/ground conductors and signal lines operating at a potential of approximately 1–5 V and spaced as close as 0.05 mm. It is also desirable that the liquid's dielectric constant be close to unity to avoid introducing significant propagation delays. Furthermore, such coolants must be nontoxic and chemically inert. Table 1 presents the thermophysical properties of the candidate fluids. The perfluorocarbons (FCs) and hydro-fluoro-ethers (HFEs) made by the 3M Corporation [3] provide this mix of properties, along with very low wetting angles on most engineering surfaces and relatively low critical pressures, thermal conductivities, and specific heats, but air solubilities approaching 50% by volume, some 25 times higher than in water [3]. The fluorocarbon liquid FC-72 (T_{sat} = 56 °C at 101.3 kPa) has been successfully used for single-phase forced convection cooling of chips in the Cray-2 super computer and for evaporative spray cooling of the Cray SV-2 module while FC-77 (T_{sat} = 97 °C at 101.3 kPa) has been used for jet impingement cooling of chips dissipating nearly 90 W/cm^2 in the SS-1 supercomputer [13].

Table 1 Thermophysical Properties of Dielectric Liquids at Atmospheric Pressure [35]

Property	FC-40	FC-72	HFE-7100	HFE-7200	Water
T_{sat} (°C)	156	56	61	76	100
ρ_f (kg/m^3)	1870	1623	1500	1430	957.8
ρ_v (kg/m^3)	25	12.7	9.6	9.26	0.5956
μ_f (mN m/s^2)	3.54	0.457	0.61	0.61	0.279
C_{pf} (J/kg K)	-	1097.8	1180	1210	4217
k_f (W/mK)	-	0.052	-	-	0.68
h_{fg}(kJ/kg)	711.6	84.97	125.6	122.6	2257
σ_f (N/m)	0.016	0.0084	0.014	0.014	0.0589
P_{cr} (kPa)	1176.0	1840.0	-	-	22100

V. POOL BOILING

While boiling heat transfer encompasses a variety of thermal transport phenomena, it is the highly efficient nucleate boiling regime [section CD in Fig. 3(a)]—in the range of 1–20 W/cm^2 heat flux and 1–20 K superheat for the FC liquids—that is of primary interest for thermal control of high heat flux electronic and microelectronic components. This regime lies between boiling incipience, associated with the initial generation of a steady stream of vapor bubbles from distinct nucleation sites, and the peak nucleate boiling heat flux, or critical heat flux, associated with vapor blanketing of the heated surface. In established nucleate boiling, large variations in heat flux can be accommodated with small variations in surface temperature.

To maintain operating chip temperatures in the preferred range of 65 °C–125 °C, the saturation temperature of the immersion cooling liquids, at atmospheric pressure, must be moderate. Several perflourinated (FCs) and hydroflouroether (HFE) fluids possessing such properties were discussed in the previous section. These properties combine to yield nucleate boiling superheats similar to those of conventional coolants (5 K–20 K) but result in

anomalous boiling incipience phenomena and in relatively modest peak heat fluxes. The low surface tension of these liquids contributes to near-zero contact angles on most known surfaces and interferes with the trapping and preservation of vapor and/or gas in surface cavities essential to heterogeneous nucleation. As a result, incipience superheats of 20 K–30 K and even as high as 72 K, have been encountered in ebullient heat transfer to these liquids. Alternately, their high gas solubility, approaching 50% by volume at standard temperature and pressure, can lower the saturation temperature of the gassy liquid by as much as 20 K.

In view of the temperature constraints imposed on individual chips and package arrays, the widespread implementation of ebullient immersion cooling for electronic systems appears to require a detailed understanding of the controlling thermal transport mechanisms and predictive relations for boiling incipience, established nucleate boiling, and the peak nucleate boiling heat flux for immersed components.

Boiling Incipience: Although it is very difficult to predict incipience overshoot, You *et al.* [18] has presented a comprehensive investigation of the parameters which affect nucleate boiling incipience for the highly wetting dielectric coolants. When the radius of the largest trapped bubble embryo is known, the following equation can be used to obtain an engineering estimate of the incipience temperature excursion ΔT_{ex}

$$\Delta T_{ex} = T_w - T_{sat}(P_l) = T_{sat}(P_b) - T_{sat}(P_l) \qquad (1)$$

where $P_b - P_l = 2\sigma_w / r_b$.

Once nucleate boiling initiates on the component, the relationship between the component heat flux and the surface superheat, i.e., its temperature rise above that of the coolant saturation temperature, is given by the Rohsenow correlation [19]

$$q = \mu_l h_{fg} \left[\frac{g(\rho_l - \rho_v)}{\sigma} \right]^{0.5} \left(\frac{c_{P,l} \Delta T_e}{c_{s,f} h_{fg} \, \mathrm{Pr}^n} \right)^a \qquad (2)$$

where $c_{s,f}$ and n are constants derived from experimental findings. The Prandtl number exponent a has been found to equal 1.7 for FC-72 [9]. In a 1987 study of perflourinated liquids and R113, with saturation temperatures ranging from 30 °C to 100 °C, Danielson *et al.* [10] found the saturated nucleate boiling characteristics of various fluorocarbons to vary widely on different platinum wire segments but to be nearly identical for a common wire segment. The results for each heater surface were found to be well correlated by the Rohsenow relation (2), with $a = 0.333$ and c_{sf} varying from 0.003 to 0.0093 for different surfaces over the entire nucleate boiling regime. However, when attention is focused on the most efficient low-heat flux nucleate boiling domain, a value of the exponent a in the range of 0.15 to 0.25 and slightly higher values of c_{sf} (0.0032 to 0.0095) appear to be more appropriate.

A. Critical Heat Flux (CHF)

The earliest theoretical models for CHF are attributed to Kutateladze [20] and Zuber [21]. Noting the similarity between "flooding" in distillation columns and the CHF condition, Kutateladze [20] obtained an expression for CHF based on a similitude analysis of the momentum and energy equations governing the two-phase flow near the heated surface. Subsequently, Zuber [21] derived an analytical equation for CHF by assuming that the Taylor hydrodynamic instability between up-flowing vapor columns and down-flowing liquid columns was the controlling mechanism [see Fig. 3(b)]. This analysis yielded the following relation for CHF:

$$q_{CHF} = \frac{\pi}{24} h_{fv} \sqrt{\rho_v} \left[g \sigma_f (\rho_f - \rho_v) \right]^{1/4}. \qquad (3)$$

Equation (3) was derived for a specific configuration, namely the saturated pool boiling of a liquid on an infinite upward-facing horizontal plate. Despite these limitations, as well as the absence of direct proof for the association of CHF with Taylor instabilities, it has been found possible to successfully apply (3) to the prediction of pool boiling CHF in a wide variety of situations. Moreover, in the ensuing years, other investigators have introduced several correction factors to extend the range of applicability of (3) by accounting for the effects of specific parameters, such as subcooling and heater geometry.

Photographic studies by Gaertner and Westwater [22] and Gaertner [23] failed to establish the predominance of vertical bubble coalescence and suggested the possibility that CHF might occur when bubbles merge laterally, forming large "mushrooms" or slugs of vapor which blanket the surface and are periodically swept away by buoyancy and/or drag forces exerted by the liquid. The periodic formation and departure of such vapor structures, depicted in Fig. 4, is at the heart of the "macrolayer" model proposed by Haramura and Katto [24].

Haramura and Katto [24] proposed that CHF is the heat flux at which the underlying macrolayer of liquid is completely evaporated in one hovering period. However, the vapor fraction at the heater surface was evaluated from the Kutateladze–Zuber expression for CHF. Consequently, the CHF values predicted using the Haramura and Katto model are identical to those obtained from (3). The

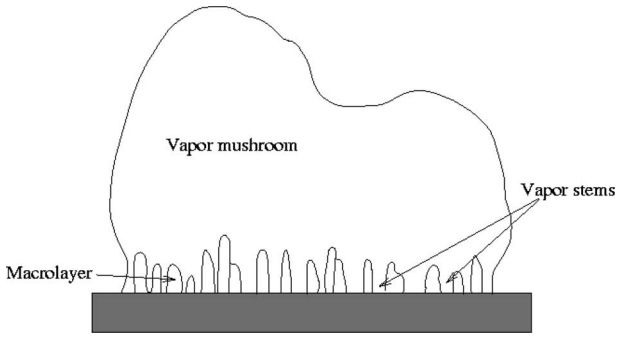

Fig. 4. ***Vapor mushroom configuration [24].***

primary contribution of this model lies in the altered view of the fluid mechanics controlling CHF, focusing not on Taylor instabilities but rather the periodic formation and removal of vapor mushrooms from the heated surface.

While the Kutateladze–Zuber and Haramura–Kato models predict CHF accurately for boiling on large, thick, well-wetted heater surfaces, these models completely ignore the effects of heater thermal properties and length scale. Early visual observations of pool boiling by Kirby and Westwater [25] and Van Ouwerkerk [26] had shown that dry patches on a heater can be rewet by the liquid after the departure of the vapor mushroom. Thus, macrolayer evaporation and local surface dryout, as proposed by Haramura and Katto [24], are not sufficient to cause CHF. Rather, building on the model of Haramura and Katto [24] and following Ramilson and Lienhard [27], for CHF to occur, it appears necessary for the temperature of the dry patch to reach the Leidenfrost point beyond which liquid–solid contact (and, hence, rewetting) is no longer possible.

More recently, Theofanous *et al.* [28] have recorded the heater surface temperature variations, as well as photographically capturing the hydrodynamic behavior of the vapor and liquid above the heater. In their experiments, Theofanous *et al.* [28] identified the occurrence of both reversible and irreversible dry spots. The authors were able to correlate the occurrence of CHF with the appearance of irreversible dry spots. Additionally, they noted the shrinkage of dry spots that was attributed to heater cool down due to radial conduction of heat away from the dry spot. These studies clearly point to the fact that the onset of CHF is not just a hydrodynamic instability phenomenon, but it reflects, as well, the contribution of thermal diffusion in the heater wall.

A comprehensive review of the effects of heater properties and length scale effects is provided by Bar-Cohen *et al.* [29]. This review paper also discusses in detail the influence of parameters such as pressure, subcooling, and dissolved gas, all of which individually appear to enhance the critical heat flux. Based on work performed by Watwe *et al.* [30], the following composite equation to predict the combined effects of pressure, subcooling, and heater properties were proposed:

$$q_{\mathrm{CHF}} = \left\{\frac{\pi}{24} h_{\mathrm{fv}} \sqrt{\rho_v}\left[\sigma_f g(\rho_f - \rho_v)\right]^{1/4}\right\} \times \left\{\frac{s}{s+0.1}\right\} \times \{1 + \langle a - \mathrm{bL}'(P)\rangle\} \times \left\{1 + b\left[\left(\frac{\rho_f}{\rho_v}\right)^{0.75} \frac{c_f}{h_{\mathrm{fv}}}\right]\Delta T_{\mathrm{sub}}\right\} \quad (4)$$

where $l' = l\sqrt{g(\rho_f - \rho_v)/\sigma_f}$ and $s = \delta_h\sqrt{\rho_h c_h k_h}$.

The first term on the right side of (4) represents the classical Kutateladze–Zuber prediction, which is the upper limit saturation value of CHF on very large horizontal heaters. The second term is the effect of heater thickness and thermal properties. The third term accounts for the influence of the length scale on the CHF and is equal to unity or higher. If the expression between $\langle\ \rangle$ is a negative number, it must be set to zero. The last term represents the influence of subcooling on CHF. Following [30], the constants a and b in (4) have the values 0.3014 and 0.01507, respectively, for horizontal heaters immersed in dielectric coolants. Similarly, the constant B in (4) has the value 0.03 for horizontal heaters and 0.043 for vertical heaters immersed in dielectric coolants. The composite TME correlation given by (4) can be used to predict the critical heat flux in a variety of situations by using the appropriate constants a, b, and B.

A comparison of experimental results in dielectric fluids to the predictions from (4) is presented in Fig. 5. The TME pool boiling CHF correlation can be used for horizontal square heaters and embodies an assumed dependence of CHF on the product of the heater thermal effusivity and thickness S [31]. Fig. 5 compares experimental data for the perflourinated FC and Novec liquids to the CHF values predicted by the TME correlation. It is found that the TME correlation can predict the pool boiling critical heat flux with a standard deviation of 12.5% for various heater materials and geometries, $0.2 < s < 120$, and in a large range of subcooling and pressure (0–75 K, 100–450 kPa) conditions, within a 95% confidence level for all except the Novec liquids, HFE7100 and HFE7200 [32]. The relatively limited thermophysical property data for the Novec liquids was blamed for this discrepancy.

It is to be noted that while the latent heat of vaporization affects nearly every phenomenon in boiling heat transfer, the impact of low latent heat values encountered in the candidate immersion cooling liquids is most pronounced in the peak nucleate boiling flux. Due to its linear dependence on the latent heat of vaporization, the saturated, pool boiling, peak heat flux for the inert dielectric liquids at near atmospheric pressure is in the

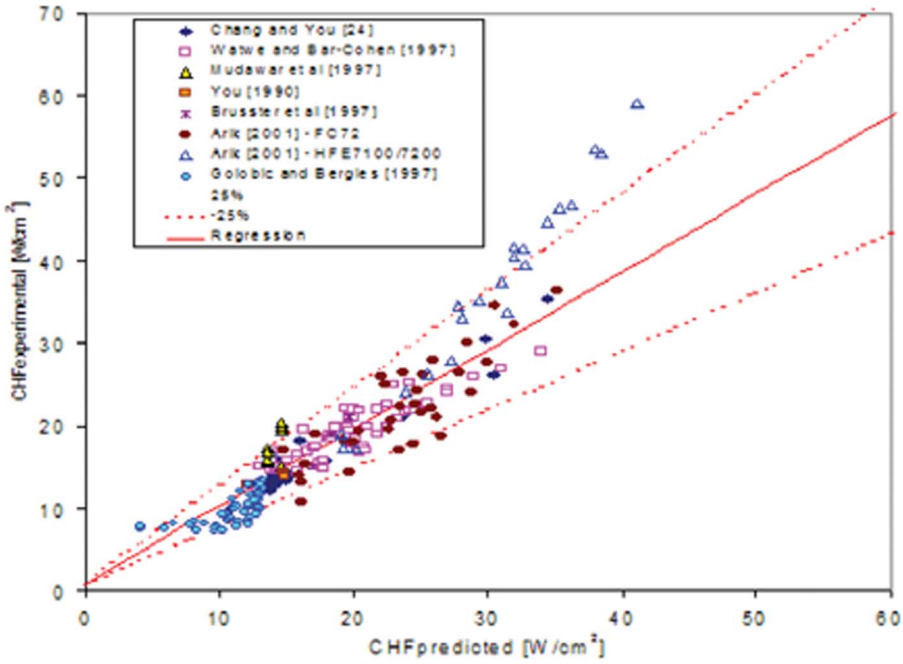

Fig. 5. *Comparison of experimental data with predictions from composite CHF equation.*

range of 15–25 W/cm^2 versus 100–120 W/cm^2 for water under similar conditions. However, unlike with water, enhancement of CHF by subcooling is very pronounced for these dielectric liquids, contributing to CHF values as high as 70 W/cm^2, as seen in Fig. 5, for high subcooling and elevated pressures.

Arik and Bar-Cohen [33] also presented the results of an experimental ebullient cooling study of chip packages immersed in the Novec dielectric liquids for a broad range of pressures and bulk temperatures. CHF values at the saturation temperatures of HFE-7100 and HFE-7200 were found to be higher than FC-72. The highest passive pool boiling CHF values for both HFE-7100 and HFE-7200 were observed at 3 Bar and 21 °C, and 53 and 59 W/cm^2, respectively. These results are an average of 50% higher than the CHF values in FC-72. TME correlation has been shown to successfully predict the observed CHF behavior for FC-72 and HFE-7100 with a low error. However, the HFE-7200 CHF values were not predicted as well. Some of this discrepancy can be related to the uncertainty in HFE fluid thermal properties [33].

The need to further raise the pool boiling CHF in electronic cooling applications has turned attention to the use of binary mixtures of dielectric liquids, with the expectation that the addition of a liquid with higher saturation temperature, higher molecular weight, higher viscosity, and higher surface tension could lead to significant enhancement in CHF. Improvements in CHF by as much as 60% using concentrations of 1%, 5%, and 10% (by weight), respectively, of FC-40 in FC-72 were demonstrated in [34] and [35] with PPGA and DIP chip packages immersed in the liquid mixtures at pressures ranging from 101.3 to 303.9 kPa. The authors explained the additive-driven enhancement and increase in the wall superheat by the localized depletion of lower boiling point liquid in the near-heater region, which produces more favorable thermo fluid mixture properties. It has also been argued that during the pool boiling in binary mixtures, the preferential evaporation of the more volatile component at the heated surface creates a surface tension gradient on the surface, which acts to enhance liquid motion towards the surface [36].

VI. GAS-ASSISTED EVAPORATIVE COOLING

Gas-assisted evaporative cooling (GAEC), with high-velocity gas-liquid flow in the narrow channels between populated substrates, offers distinct advantages in the thermal management of compact three-dimensional packaging of microelectronics and was successfully incorporated into a prototype high-performance computer module by Cray Research Incorporated [11].

The Cray-3 prototype module, shown in a cross-sectional view in Fig. 6, contained 16 stacks of four circuit boards, each populated by 16 GaAs flip chips, 3.9 × 3.9 mm, and dissipating up to 3 W, for a peak chip heat flux of nearly 20 W/cm^2 and an average board heat flux of 7.7 W/cm^2. Each board in the stack was separated by 0.51-mm spacers, providing a clearance of 0.1 mm from the back of each GaAs chip to the next circuit board. This

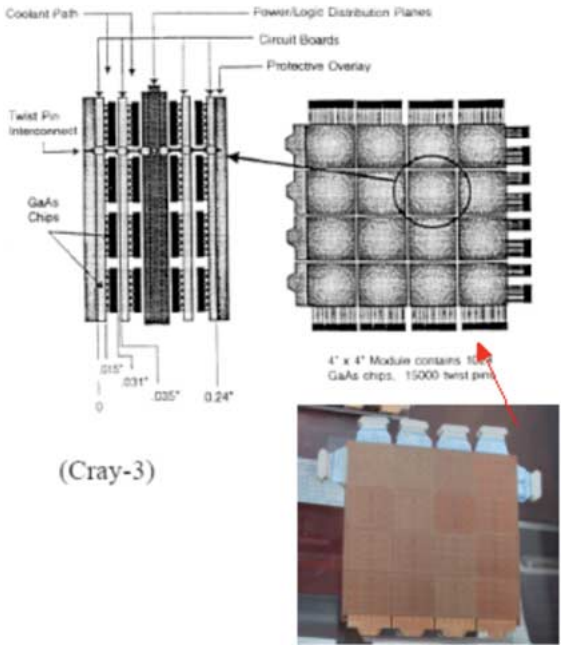

Fig. 6. ***Cray-3 module assembly [37].***

design provided for an extremely high-power density, yielding as much as 1.5 kW per logic module, of dimensions $10.1 \times 10.1 \times 0.64$ cm and approaching 18 W/cm^3 in several sections of the system. Chip temperatures were reported to average 25 °C (±8 °C) during operation of the module. Total power dissipation for a 16-processor Cray-3, comprised of 80 logic modules and 256 memory modules, was expected to approach 270 kW, including approximately 90 kW in the power supplies [37].

The cooling system developed for the Cray-3, shown in Fig. 7, was designed to minimize the mass flow of coolant through the module and to maintain a uniform temperature across the module. The desire to reduce liquid mass flow rate led to the use of gas-assisted evaporative cooling, with pressurized helium driving FC-72, sprayed over the top of the module, into the narrow channels, or microgaps of 100 μm over the GaAs chips. The module was oriented vertically, relying on gravity and a modest pressure differential of 20.6 kPa to circulate the coolant.

Based on the results reported by Bar-Cohen *et al.* [37], volumetric heat removal rates in excess of 50 W/cm^3 could be achieved in a three-dimensional (3-D) package by using helium or nitrogen-assisted flow of Fluorinert through a submillimeter channel. Detailed experimental measurements in the laboratory apparatus supported earlier findings attained with a prototype Cray-3 module using helium and FC-72. In the laboratory apparatus, a 0.5-mm GAEC asymmetrically heated channel was found to accommodate a single-wall average heat flux of 3.79 W/cm^2 with a liquid superficial velocity of 0.16 m/s and nitrogen velocity of 7.14 m/s. This configuration thus yielded a volumetric heat removal rate—based only on the channel dimension—of nearly 75 W/cm^3. The investigators concluded that substantial experimental and theoretical effort would be required to determine the limits of the GAEC technique and to optimize the GAEC technique for practical applications.

VII. JET IMPINGEMENT

Impingement cooling may involve a single jet directed at a single component or an array of electronic components, multiple jets directed at a single component, arrays of jets directed at an array of chips on a common substrate, or an array of jets directed at chip packages on a printed circuit board. The jets may be formed by circular slot-shaped orifices or nozzles of various crosssections. The space surrounding the jet may be filled with a gas, leading to a jet with a free surface. Alternately, liquid may occupy the space between the liquid distributor plate and the heated surface, leading to a submerged jet. As a final distinction, jet impingement cooling of electronic components may involve forced convection alone or localized flow boiling, with or without net vapor generation. These various jet impingement heat transfer modes will be discussed in the following sections of this paper. A typical configuration for single-phase submerged jet impingement cooling is illustrated in Fig. 8.

A. Free-Surface Jet Impingement

When a jet impinges on a surface, very thin hydrodynamic and thermal boundary layers form in the impingement region due to jet deceleration and increase in pressure. Consequently, extremely high heat transfer coefficients are

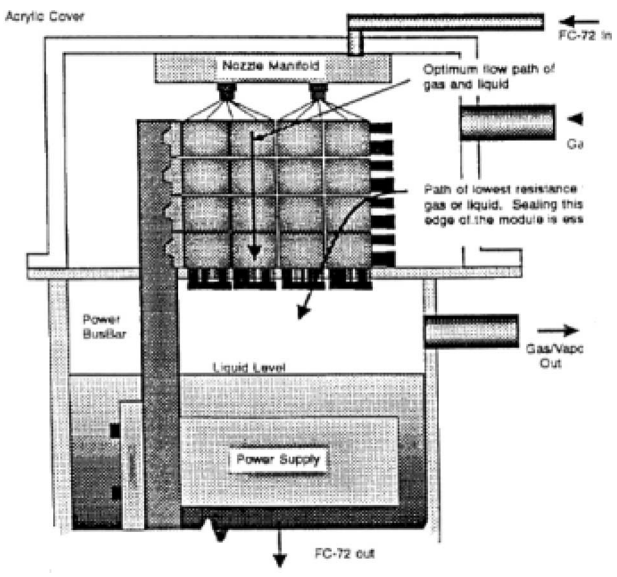

Fig. 7. ***CPU tank assembly [37].***

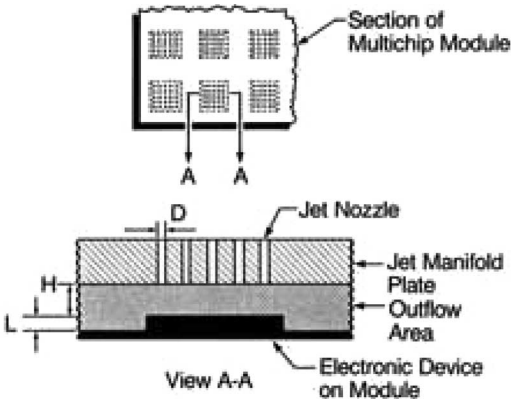

Fig. 8. *Typical configuration for submerged jet impingement cooling.*

obtained within the stagnation zone. Since the peak heat transfer only occurs within the stagnation zone, a single impinging jet can provide effective heat transfer when highly localized heating or cooling is required.

As shown in Fig. 9, the flow in a jet impinging perpendicularly on a plate surface is commonly divided into three separate regions: the free region, the impingement region, and the radial flow region.

The flow in the free jet zone is mainly in the axial direction and is not affected much by the presence of the impingement surface. Within this free jet zone, there are two subregions, the potential core with velocity equal to the jet exit velocity and a free surface jet flow with a lower velocity shear layer, which is slowed by the drag and entrainment of the surrounding fluid. Downstream from the nozzle, the shear layer progressively expands into the potential core, eventually reaching the jet centerline. In the stagnation flow region, the flow impinges on the surface and then turns, flowing parallel to the surface. The parallel flow portion is called the wall-jet region. Depending on the temperature of the liquid in the jet (saturated or subcooled) and the temperature difference between the target wall temperature and the saturation temperature of the jet liquid, impingement heat transfer may provide either single-phase or two-phase cooling.

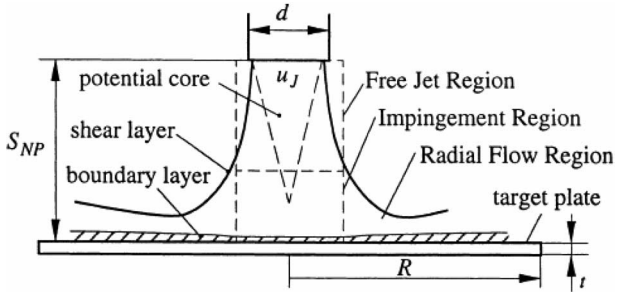

Fig. 9. *Schematic of single impinging jet.*

Since impinging jets can provide very high local heat transfer rates, this technique has been used in a variety of practical engineering applications, such as quenching of metals and glass, cooling of turbine-blades, cooling and drying of paper, and more recently cooling of high heat flux electronics. Many studies have dealt with the heat transfer characteristics and performance limits of impinging jets for both single-phase [38], [39] and two-phase [40] thermal transport.

B. Convective Jet Impingement

In general, the surface–convection resistance is the smallest in the stagnation-flow region and increases in the wall-jet region. Several distinct approaches have been used to describe impinging jet heat transfer, including:

1) theoretical analysis for the wall-jet region, based on boundary-layer approximations [41]–[43];
2) direct CFD numerical simulations of the continuity equation, the momentum equations, and the energy equation with the appropriate boundary conditions and/or turbulent models [44]–[46];
3) systematic experimental investigations performed to obtain the impingement heat transfer rate with different working fluids ($0.7 < \mathrm{Pr} < 450$) and operating conditions [39], [47], [48].

These investigations have provided an understanding of the structure of the jet flow and the resulting heat transfer characteristics and forces on the flat surface by relating them to the geometric and dynamical features of the jet, especially the large-scale coherent structures, which are the main phenomena controlling momentum and heat transport in jets.

It is well established that that the average heat transfer coefficient over the impingement surface (see Fig. 9) depends on parameters such as the jet Reynolds number Re, nozzle-to-plate distance s_{NP}, nozzle geometry d, the impinging wall geometry R, and the inlet coolant Prandtl number Pr. Several recent and classical correlations are reviewed in the following.

Convective Single-Jet Impingement: One of the most widely used correlations for the average Nusselt number in a single-jet impingement is due to Martin and takes the following form [49]:

$$\mathrm{Nu}/\mathrm{Pr}^{0.42} = g(d/r, s_{\mathrm{NP}}/d) f(\mathrm{Re}_J)$$
$$f(\mathrm{Re}_J) = 2\mathrm{Re}_J^{1/2}\left(1 + \frac{\mathrm{Re}_J^{0.55}}{200}\right)^{0.5}$$
$$g(d/r, s_{\mathrm{NP}}/d) = \frac{d}{r}\frac{1 - 1.1d/r}{1 + 0.1(s_{\mathrm{NP}}/d - 6)d/r} \qquad (5)$$

where Re_J and Nu are the Reynolds number and the Nusselt number based on the nozzle diameter

$$\mathrm{Re}_J = \frac{u_J d}{\nu} \quad \mathrm{Nu} = \frac{\mathrm{hd}}{k_f} \tag{6}$$

and where h is the average heat transfer coefficient based on the average temperature difference between the target and the coolant.

The range of validity for this correlation, developed from extensive gas jet data, as well as some data for water and other higher Pr number liquids, and including some high Schmidt number mass transfer data, is given by Martin [49] as: $2 \times 10^3 \leq \mathrm{Re}_d \leq 10^5$, $0.6 < \mathrm{Pr(Sc)} < 7(900)$, and $2 \leq H/D \leq 12$. Martin found this correlation to provide a predictive accuracy of 10%–20% over the stated parametric range. The average Nu was also found to be nearly unaffected by the angle of inclination of the jet [63]. It is to be noted that for jets produced by sharp-edged orifices, jet contraction immediately after the orifice exit must be taken into consideration in calculating the average velocity, jet diameter, and nozzle area ratio f.

The general form of the equation for the local Nu number at the stagnation zone has been well established both for submerged and free surfaced jets by Sun *et al.* [48]

$$\mathrm{Nu}_0 = 1.25\,\mathrm{Pr}^{1/3}\,\mathrm{Re}^{1/2}. \tag{7}$$

The exponent of the Re number clearly indicates the laminar characteristic of impingement flow in the stagnation zone. Further solutions for an impinging laminar jet on a horizontal surface at arbitrary heat-flux conditions were derived using an integral technique [43].

Convective Multiple-Jet Impingement: The heat transfer rate for multiple-jet impingement can be estimated from the single-jet impingement case by allocating a "unit cell" on the heated surface to each one of the jets. If the interaction between adjacent jets within the representative area and the influence of the spent fluid flow is neglected, the heat transfer data inferred from a single jet can approximately represent the actual situation. In this respect, the relative nozzle area α_J is defined as the ratio of the nozzle exit cross section to the impact or influence area of a single jet a_r

$$\alpha_J = \pi d^2/4a_r \tag{8}$$

for the single jet $d/r = 2\sqrt{\alpha_J}$. The correlation equation for an array of nozzles may be obtained from the single nozzle (5) by replacing d/r with a term related to the relative nozzle area α_J. In the range of $0.004 \leq \alpha_J \leq 0.04$, the geometric function G for the arrays of nozzles thus becomes

$$g(\alpha_J, s_{\mathrm{NP}}/d) = 2\sqrt{\alpha_J}\,\frac{1 - 2.2\sqrt{\alpha_J}}{1 + 0.2(s_{\mathrm{NP}}/d - 6)\sqrt{\alpha_J}}. \tag{9}$$

However, the influence of nozzle-to-plate spacing s_{NP} also needs to be accounted for. The above simple replacement gives a sufficiently accurate result for widely spaced jets $(s_{\mathrm{NP}}/d)_{\mathrm{lim}}$. When the jets are more closely positioned, jet-to-jet interactions increase, and the heat transfer coefficient thus begins to decrease. Consequently, the optimum distance, yielding the highest heat transfer rates, can be expressed as a function of the relative nozzle area α_J and is empirically found as [49]

$$(s_{\mathrm{NP}}/d)_{\mathrm{lim}} = 0.6/\sqrt{\alpha_J}. \tag{10}$$

The degradation of the heat transfer due to the interaction between the adjacent jets can be incorporated into the single-jet equation by an empirical correction function K. It can be given as a single expression

$$k(s_{\mathrm{NP}}/d, \alpha_J) = \left[1 + \left(\frac{s_{\mathrm{NP}}/d}{0.6/\sqrt{\alpha_J}}\right)^6\right]^{-0.05}. \tag{11}$$

The function f, given in (5), which describes the effect of the Re number, is prescribed for single-jet impingement. The Re function f, for arrays of nozzles, is empirically correlated by

$$f(\mathrm{Re}_J)_{\mathrm{AN}} = 0.5\mathrm{Re}_J^{2/3} \quad (2000 < \mathrm{Re}_J < 100\,000). \tag{12}$$

Therefore, the heat transfer coefficient for an array of nozzles based on the modifications of the related correlation equation for single nozzle is given as

$$\left(\frac{\mathrm{Nu}}{\mathrm{Pr}^{0.42}}\right)_{\mathrm{AN}} = \mathrm{Re}_J^{2/3}\left[1 + \left(\frac{s_{\mathrm{NP}}/d}{0.6/\sqrt{\alpha_J}}\right)^6\right]^{-0.05} \times \frac{\sqrt{\alpha_J}(1 - 2.2\sqrt{\alpha_J})}{1 + 0.2(s_{\mathrm{NP}}/d - 6)\sqrt{\alpha_J}}. \tag{13}$$

The above correlation is valid in the range of $2000 < \mathrm{Re}_J < 100\,000$, $0.004 < \alpha_J < 0.04$, and $2 < s_{\mathrm{NP}}/d < 12$ [49].

Phase-Change Jet Impingement: In the absence of boiling, a free jet forms a radial wall jet that emanates from the

impingement zone while remaining mostly in contact with the heated wall. Unlike the situation with single-phase jet impingement cooling, during boiling along the heated surface, the vigorous, at times explosive, generation of vapor bubbles within the wall jet splashes away a significant portion of the wall jet liquid flow. Further increases in heat flux result in the formation of dry patches in the outer circumference of the wall jet, as much of the wall jet liquid is splashed away in these outer regions. Eventually, this dryout propagates inwards toward the impingement zone, causing separation of the wall jet from much of the heated wall and resulting in dryout/CHF, as illustrated in Fig. 10 [50].

Due to the existence of different boiling regimes, which depend on surface temperature and geometry as well as coolant flow conditions and subcooling, boiling from high temperature surfaces experiencing liquid jet impingement can be quite complex. The physics governing the heat removal process by boiling jets is still not completely understood and few theoretical models are available in the literature.

Early experimental studies on impingement boiling from a simulated microelectronic chip were performed by Ma and Bergles [51] with single submerged R113 jets (1070 μm in diameter) impinging onto a vertical heater (5×5 mm) in saturated and subcooled conditions. Numerous experimental investigations with boiling free jets have been reported for a range of impact velocities, ratios of liquid density to vapor density, and multiple jet systems [52]–[58].

The focus of two-phase jet impingement cooling studies has been the determination of CHF. It has been determined that CHF for free circular jets can be enhanced by increasing jet velocity or decreasing jet diameter [50]. For a confined rectangular impinging jet of dielectric liquid FC-72 on a simulated electronic chip, jet velocity has a stronger effect on CHF than jet width [59]. An enhancement of over 300% in CHF was achieved when impingement velocity was increased from 1 to 11 m/s. Thus, the coolant flow rate requirements for rectangular jets can be reduced by choosing a smaller jet width, as is the case for single-phase jet impingement heat transfer. Dramatic CHF enhancement was also achieved by increasing the subcooling of the liquid. Higher subcooling was especially beneficial in condensing the vapor bubbles in the radial wall jet, thus greatly delaying the wall jet separation and the resulting dryout, caused by the bubble growth.

Studies of submerged jets have recognized that there are two types of behavior in jet impingement boiling [60]–[63].

1) Nucleate boiling, in which bubbles are formed by nucleation at the solid surface washed by the impinging jet. In saturated boiling, these bubbles grow, detach, and join the main two-phase flow. In highly subcooled boiling, they collapse rapidly while heating the main liquid flow towards the saturation temperature.
2) Convective boiling, or thin-film evaporation, in which heat is transferred by conduction and convection to the liquid/vapor interface, sometimes assisted by bubble dynamics. Two-phase jet impingement on a flat hot plate can be further divided into two modes, the free film flow and the stagnation jet flow. In steady-state jet impingement boiling, the dryout or the critical heat flux ($q_{\mathrm{CHF,sat}}$) generally occurs at the downstream location furthest from the stagnation point, and data for $q_{\mathrm{CHF,sat}}$ are typically correlated in terms of the heat source dimension (2R). One widely accepted correlation developed for a saturated jet is of the form [64]

$$\frac{q_{\mathrm{CHF,sat}}}{\rho_g h_{\mathrm{fg}} u_J} = 0.221\left(\frac{\rho_f}{\rho_g}\right)^{0.645}\left[\frac{2\sigma}{\rho_f u_J^2 (2r-d)}\right]^{-0.343} \times \left(1+\frac{2r}{d}\right)^{-0.364}. \quad (14)$$

For the CHF of subcooled liquids for forced convective boiling, the following form is frequently applied [65]:

$$\Phi = \frac{q_{\mathrm{CHF,sub}}}{q_{\mathrm{CHF,sat}}} = 1+\varepsilon_{\mathrm{sub}}$$

$$\varepsilon_{\mathrm{sub}} = 0.952\left(\frac{\rho_f}{\rho_g}\right)^{0.118}\mathrm{Ja}^{1.414}$$

$$\mathrm{Ja} = \frac{c_{P,f}(T_{\mathrm{sat}}-T_{\mathrm{bulk}})}{h_{\mathrm{fg}}}. \quad (15)$$

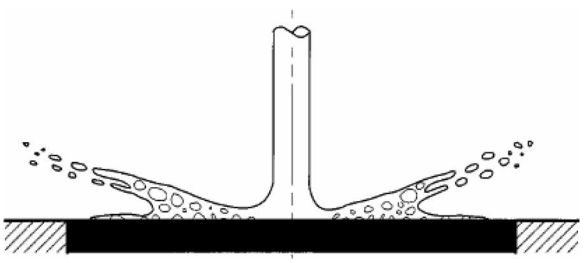

Fig. 10. *Liquid wall layer splashing and separation in free circular impinging jets [50].*

Recently, a semitheoretical correlation for the CHF of saturated water jet impingement boiling of mode B

(convective boiling) was proposed [66]

$$\frac{q_{\mathrm{CHF,sat}}}{\mathrm{Gh_{fg}}} = 0.132\left(1+\frac{\rho_g}{\rho_f}\right)^{1/3}\left(\frac{\sigma\rho_f}{g^2 d}\right)^{1/3}\left(\frac{\rho_g}{\rho_f}\right)^{1.4/3} \tag{16}$$

where G is the jet liquid mass flux in kilograms per meters squared per second.

It is to be noted that for specified fluid and operating conditions, this relation can be simplified by inserting the thermophysical properties, as shown in (17), for water at atmospheric pressure

$$q_{\mathrm{CHF,sat}} = 0.36\times 10^6\left(\frac{u_J}{d}\right)^{1/3}. \tag{17}$$

For the CHF of subcooled liquids for forced convective boiling, the following form is often applied:

$$\frac{q_{\mathrm{CHF,sub}}}{q_{\mathrm{CHF,sat}}} = 1 + c\left(\frac{\rho_g}{\rho_f}\right)^n\left(\frac{c_{P,f}\Delta T_{\mathrm{sub}}}{h_{\mathrm{fg}}}\right)^{\mathrm{m}} \tag{18}$$

where c, m, and n would be determined by the experimental data. One recent empirical correlation was recommended for subcooled water jet impingement at the stagnation zone under atmospheric pressure [67]

$$\frac{q_{\mathrm{CHF,sub}}}{q_{\mathrm{CHF,sat}}} = 1 + 11.82\left(\frac{c_{P,f}\Delta T_{\mathrm{sub}}}{h_{\mathrm{fg}}}\right). \tag{19}$$

Both the impact velocity and the nozzle diameter have a relatively strong effect on the CHF of subcooled water. As shown in (19), the CHF of saturated water is of the form $q_{\mathrm{CHF,sat}}\alpha(u_J/d)^{1/3}$. The same relationship of $q_{\mathrm{CHF,sub}}\alpha(u_J/d)^{1/3}$ is also found for subcooled water. However, the general correlation for other liquid jet boiling is still under development.

Submerged Jet Cooling of Electronics: In applying the Martin correlation (13) to the cooling of electronic components constituting discrete heat sources on a large surface, it is necessary to alter the definition of the jet area ratio α_J. Recognizing that, in this application, the impingement area is usually equal to the component area, the jet area ratio α_J can be expressed as

$$\alpha_J = \left(n\frac{a_{\mathrm{jet}}}{a}\right) = 0.785 d^2\frac{n}{a}. \tag{20}$$

One factor which may need to be considered in application of the Martin correlation is the effect of escaping cross flow at the perimeter of a chip or board. As the velocity of the escaping flow increases relative to the jet velocity, the cross-flow effect can become more significant.

In applying this correlation to the submerged jet cooling of electronic components, as described, for example, in [52], [60], [61], and [63], the complex variation of the nondimensional heat transfer coefficient Nu with the area ratio α_J and the jet distance s_{NP}/d may, unfortunately, mask the fundamental relationships among these parameters and obscure the primary contributors to the variation in the impingement heat transfer coefficient. Re-expressing the correlation with simplifications applicable to typical electronics cooling, the average Nusselt number is found to be approximately equal to

$$\mathrm{Nu}_d \cong 0.5\left(\frac{h}{h}\right)^{-0.3}\alpha_J^{0.35}\mathrm{Re}_d^{0.667}\,\mathrm{Pr}^{0.42}. \tag{21}$$

This approximation falls within 30% of the original Martin correlation throughout the parametric range of the correlation but provides values within 10% of (13) for $s_{\mathrm{NP}}/d < 3$ and close to that value in the primary parametric range of interest.

Recalling the definition of the jet Nu number (i.e., Nu = hD/k) and substituting for the area ratio α_J, the heat transfer coefficient produced by impinging liquid jet(s) is found to be proportional to

$$h \propto \mathrm{kH}^{-0.3}(\mathrm{n/A})^{0.35}\mathrm{Re}_d^{0.667}\,\mathrm{Pr}^{0.42} \tag{22}$$

or, expanding the Re and Pr numbers

$$h \propto \left[k^{0.58}\rho^{0.67}\mu^{-0.25}\right]\left[(\mathrm{n/A})^{0.35}d^{0.67}\right]\left[h^{-0.3}\nu^{0.67}\right]. \tag{23}$$

Following [63], the first bracketed term represents a fluid figure-of-merit for submerged-jet heat transfer, the second term constitutes a thermal figure-of-merit for the jet plate, and the third, the operating conditions of an impingement cooling system.

Clearly, to maximize the jet heat transfer rate, it is desirable to choose a liquid with high thermal conductivity and density but relatively low viscosity. The ideal jet manifold would contain many large-diameter nozzles per component. Fig. 11 displays this trend for 16-jet arrays, showing the heat transfer coefficient increasing from 16.5 kW/m^2k for a jet diameter of 0.27 mm to 17.8 kW/m^2k at 0.32 mm. Due to the strong dependence of the heat transfer rate on the jet Reynolds number,

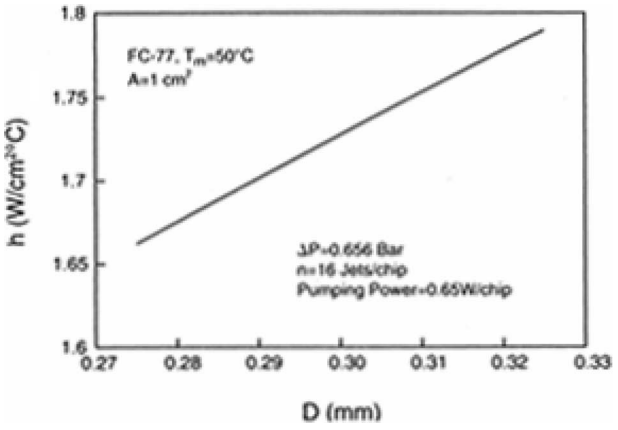

Fig. 11. *Sensitivity of average heat transfer coefficient to change in jet diameter at constant nozzle pressure drop [63].*

maximization of the heat transfer coefficient also requires increasing the liquid velocity at the nozzle and decreasing the distance of separation between the nozzle and the component. Alternately, if a liquid has been selected and if the jet Reynolds number is to remain constant, a higher heat transfer coefficient can only be obtained by increasing n/A or decreasing s_{NP}.

Although the thermal relations discussed in the previous section can be used to establish the gross feasibility of submerged jet impingement cooling for high-power chips, successful implementation of this thermal management technique requires consideration of system-level issues and design tradeoffs. The minimization of life-cycle costs is a crucial element in electronic systems and, consequently, attention must be devoted to the "consumed" liquid flow rate, pressure drop, and pumping power, as well as to the limitations imposed by manufacturing tolerances and costs. The gross impact of these considerations on the design of impinging jet cooling systems can be seen with the aid of (23).

From an examination of the approximate relation for the jet heat transfer coefficient, it may be seen that maintaining high heat transfer rates at low jet velocities would necessitate increasing the number of nozzles (n/A), increasing the diameter of each nozzle (D), or decreasing the spacing between the nozzle exit and the component (s_{NP}). The minimum spacing value is likely to be determined by the precision of assembly and deflection under pressure of the jet-plate and, thus, will benefit from reduced operating pressure. Since the maximum heat transfer rates are approached asymptotically as the total jet area increases to approximately 4% of the component area, there is coupling between the number of jets and the jet diameter. The heat transfer rate can, thus, be improved by increasing both jet diameter and the number of jets up to this value, but if operating near the maximum rate, the jet diameter is inversely related to the square root of n/A.

These results suggest that optimum performance, based on system-level as well as thermal considerations, as represented by the average beat transfer coefficient, would be achieved by designing jet impingement systems to provide approximately 4% jet-to-component-area ratios and operate at relatively low jet velocities. Improved surface coverage, more uniform heat removal capability, and decreased vulnerability to blockage of a single (or a few) nozzles would appear to be favored by the use of a relatively large number of jets per component, allowing a reduction in the diameter of individual jets. Alternately, the cost of manufacturing and the probability of nozzle blockage can be expected to increase for small diameter nozzles and, thus, place a lower practical limit on this parameter. Unfortunately, given their approximate nature, these relationships must be viewed as indicative, rather than definitive, on these parametric trends.

Another useful test of design robustness is a plot of h versus pumping power for a given jet diameter as shown in Fig. 12. The plot shows that a 10% reduction in pumping power will result in a 6% decrease in h for values of approximately 15 kW/m^2k. If a variation in pumping power is known to exist for a given circulation system, Fig. 12 can be used to ensure that the resulting variations in h will not go below the required minimum.

Maddox and Bar-Cohen [63] concluded that the parametric relations embodied in the Martin correlation (13) point to increasing heat transfer rates with increasing Re and Pr numbers and with a decreasing jet aspect ratio. The interplay of parameters and constraints on the thermo fluid characteristics of a jet impingement cooling system was studied for a "case study," with a required heat transfer coefficient of 1.7 W/cm^2k. It was found that increasing the number of jets per chip n substantially reduced the required pumping power, especially for $n < 20$. Also, there was an optimum jet

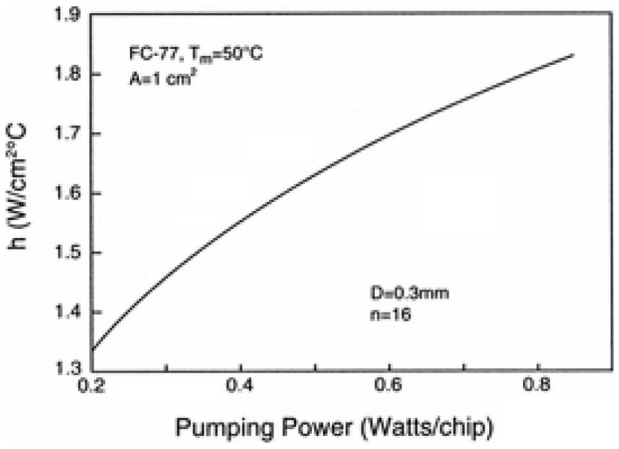

Fig. 12. *Sensitivity of average heat transfer coefficient to change in pumping power [63].*

diameter, which varied with both the number of jets per chip and the jet aspect ratio. One possible design optimization consisting of 16 jets per chip and a jet diameter of 0.3 mm would require a nozzle pumping power of 0.60 W/chip.

VIII. SPRAY COOLING

In recent years, considerable attention has been devoted to spray cooling of high heat flux chips with dielectric liquids, for example [69] and [71]. In general, spray cooling heat transfer displays three distinct domains of behavior at low, middle, and high surface temperatures, corresponding to the nucleate, transition, and film boiling regions. Spray heat transfer with dielectric liquids appears to be much more effective than saturated pool boiling, achieving peak heat fluxes that can be several times higher than saturated pool boiling CHF, though spray cooling does require the investment of significant pumping power. The temperature overshoot encountered with boiling incipience seems to be entirely eliminated by the use of liquid sprays, and spray cooling can provide a relatively uniform surface temperature. However, the cooling rates achieved in spray cooling are dependent on the liquid droplet properties and behavior.

The breakup of a droplet upon impingement on the surface is described by the droplet Weber number, We_d, which is defined as the ratio of droplet inertia forces to surface tension forces, using the droplet diameter D as the length scale and u_d the characteristic velocity of the droplet normal to the surface

$$We_d = \frac{\rho_f u_d^2 d}{\sigma}. \tag{24}$$

As an impinging droplet contacts a hot solid surface, heat is transferred from the solid to the liquid phase by conduction, convection, and radiation, increasing the temperature of the liquid or alternatively vaporizing liquid from the base of the droplet. The droplet Weber number has a strong influence on the spreading characteristics and integrity of the droplet and several distinct dynamical regimes of droplet impact associated with specific ranges of the Weber number have been recognized.

Thus, both the Weber number and the surface superheat can affect the behavior of the impinging droplets and are the spray cooling heat transfer rates. The influence of surface temperature on droplet impact dynamics was investigated in a comprehensive photographic study [72]. Flash photography was used to observe the liquid film's spreading structure and rate, vapor bubble formation, and contact angle for *n*-heptane droplets with $We_d = 43$ impinging upon a polished stainless steel surface. All these impact characteristics were highly temperature dependent over the range of 24 °C–250 °C.

Fig. 13 provides one example of the droplet impact regimes for a droplet Weber number of 20. At a given surface temperature, the history of the impact and associated heat transfer mechanisms is described by the

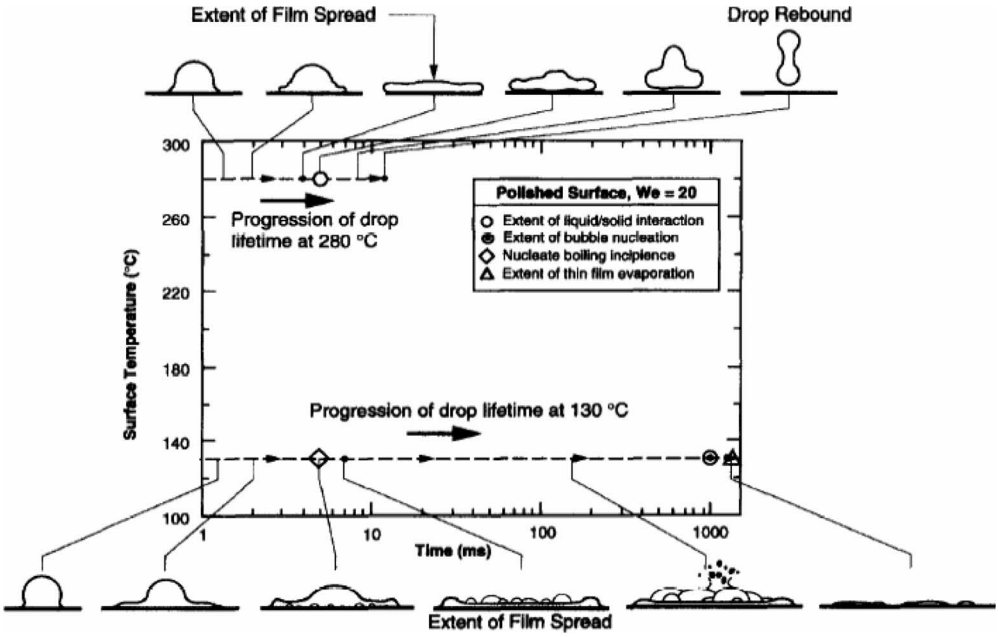

Fig. 13. *Schematic of droplet-spray impact regime temperature-time maps [73].*

corresponding boiling regimes for each of three Weber numbers. At lower surface temperatures, surface–bubble nucleation dominated the isolated impinging droplet.

The maximum heat transfer per drop impinging on hot surfaces ($q_{\max}$) was observed to be a function of the fluid properties and the normal component of the impact velocity u_d for superheats of about 165 °C for water, acetone, alcohol, and some freons. As much as 50% of the droplet mass was found to evaporate during the short time interval associated with impact and bouncing. A correlation of experimental data was given as [74]

$$\frac{q_{\max}}{\rho_d d^3} = 1.83 \times 10^{-3}\left(\frac{\rho_d^2 u_d^2 d}{\rho_\nu \sigma g}\right)^{0.341}\left[h_{\mathrm{fg}} + c_{P,\nu}\left(\frac{T_w - T_{\mathrm{sat}}}{2}\right)\right]. \quad (25)$$

Sprays can be classified into either pressure sprays or atomized sprays, depending upon the method used to accomplish the liquid breakup. Despite their superior cooling performance, atomized sprays are difficult to incorporate in a closed loop electronic cooling system because of the complexity of separating air from dielectric liquid coolants. The droplet sprays can have the form of a mist and impinge on the surface with a random pattern. After hitting the surface, the liquid droplets spread and often merge to form a thin liquid film. If the wall superheat is above the Leidenfrost point, a thin vapor layer is present underneath the droplets or the liquid film.

As shown in Fig. 14, two spray cooling regimes can be recognized: a light spray (a small volumetric flux) and a dense spray (a high volumetric flux). In a light spray, the frequency of drop impingement upon the heated surface is low, leaving much of the surface covered with fairly stagnant liquid within which vapor bubbles can easily nucleate and aid the evaporation process. Evaporation efficiency in light sprays is, therefore, very high.

The relative contributions of the various phenomena involved in spray cooling still remain unclear. Specifically, vapor bubbles on a heater surface may prematurely break up due to droplet impingement, allowing surface rewetting at a rate higher than that in pool boiling. On the other hand, the nucleation within the liquid film in spray cooling is also important [76]. Since droplets can entrain vapor and air bubbles and carry them near or to the surface, nucleation site density can be increased at a given surface temperature. However, the droplet size is important only when evaporation occurs from the liquid film deposited on the impinged surface [77].

Alternatively, it may be argued that volumetric flux is of much greater significance in characterizing spray heat transfer rates than drop velocity. Drop velocity affects the local heat transfer from the heated surface momentarily, while the volumetric flux determines the cumulative effect of multiple drop impingements [75].

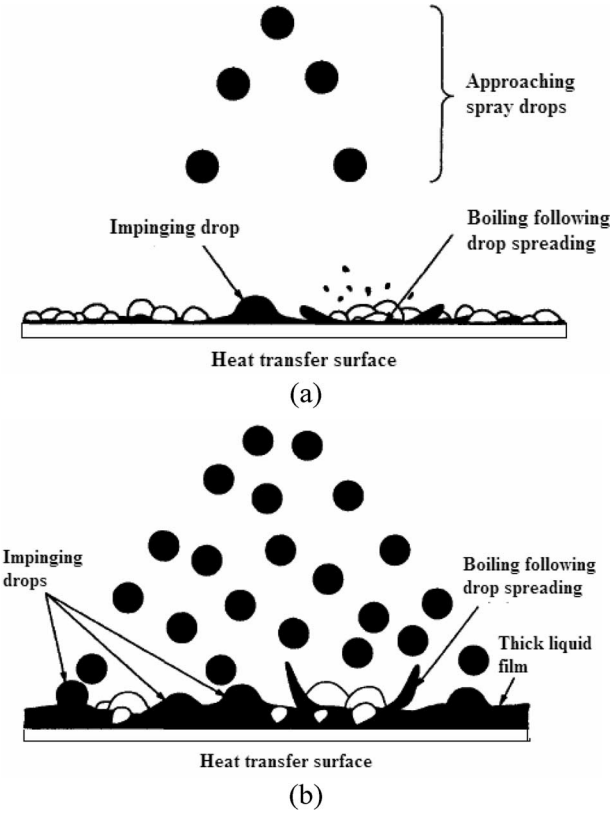

Fig. 14. *Two types of spray processes [75]: (a) light spray (low We) and (b) dense spray (high We).*

Light spray evaporative cooling in a surface-nucleation regime with small wall superheat has been studied in detail for electronic cooling applications. The CHF in spray cooling is complicated by liquid droplet impact on the thin layer of super heated liquid, which is influenced by both the boundary-layer development and a complex two-phase flow with the rapid generation and diffusion of vapor and bubbles. Correlations have been developed for CHF and heat transfer characteristics of water, FC-72, and FC-87 over a wide range of flow rates and subcoolings [75]

$$\frac{q_{\mathrm{CHF}}}{\rho_v h_{\mathrm{fg}} \dot{v}} = 2.3\left(\frac{\rho_f}{\rho_g}\right)^{0.3}\left(\frac{\sigma}{\rho_f \dot{v} d_{\mathrm{SMD}}}\right)^{0.35} \times \left(1 + 0.0019\frac{\rho_f c_{P,f}\Delta T_{\mathrm{sub}}}{\rho_v h_{\mathrm{fg}}}\right)$$

$$\frac{d_{\mathrm{SMD}}}{d} = 3.67\left[\mathrm{We}_d^{1/2}\mathrm{Re}_d\right]^{-0.259}$$

$$\mathrm{We}_d = \frac{\rho_a(2\Delta P/\rho_f)d}{\sigma}$$

$$\mathrm{Re}_d = \frac{\rho_f(2\Delta P/\rho_f)^{1/2}d}{\mu_f} \quad (26)$$

where D and d_{SMD} are nozzle orifice diameter and Sauter mean diameter (SMD), which were successfully correlated for fluids with vastly different values of surface tension. Sauter mean diameter is defined as the diameter of a drop having the same volume/surface area ratio as the entire spray. This correlation was based upon orifice diameter and the We and Re numbers of the orifice flow prior to liquid breakup. $\dot{v}$ is local volumetric flux, ΔT_{sub} is the liquid subcooling $(T_{sat} - T_f)$, and ρ_a is the density of ambient fluid (air or vapor).

A recent study on spray cooling in a closed system with different fractions of noncondensable gases found that the heat flux was dependent only on the total system pressure and remained unaffected by the partial pressure of noncondensables in the system. While the correlation matched well with the data at high pressures (101 kPa), it considerably underestimated the CHF at low system pressures (by 45% at 10.4 kPa). One possible reason is that the vapor density dependence on system pressure is not properly taken into account in the correlation. A modified correlation, incorporating the vapor density dependence on system pressure, has been developed [78].

Based on the available spray cooling literature, it can be concluded that while spray and jet impingement provide similar heat transfer coefficient and critical heat flux values—for similar pumping power, volume, and cost—liquid spray results in a more uniform temperature profile on the heater surface [50] and avoids the premature dryout encountered in jet-impingement cooling due to the separation of the wall liquid layer during vigorous boiling. However, the adoption of spray cooling has been constrained by concerns over inconsistent spray characteristics, erosion, and clogging in the nozzles due to the very small orifice diameter and high pressure required to produce small droplets.

IX. SYNTHETIC JETS FOR DIRECT LIQUID COOLING

Synthetic jets are intense small-scale turbulent jets formed from periodic entrainment and expulsion of fluid by microfluidic devices immersed in the liquid. The jets can be made to impinge upon electronic components, thereby providing forced convection impingement cooling. The small size of these devices, accompanied by the high exit velocity of the fluid, provides an opportunity to significantly reduce the volume of the hardware used for the thermal management of electronics [79], [80].

Synthetic jet enhancement of natural convection and pool boiling heat transfer in an enclosure, filled with a dielectric, electronic cooling liquid (FC-72), was studied in [81]. The jet actuator used in this paper produced planar submerged liquid jets that impinged upon a flat foil heater and spread laterally along its surface. Both natural convection and pool boiling experiments have been performed to obtain the heat transfer enhancements.

A. Natural Convection

For the natural convection experiments the heat flux was kept constant at 0.37 W/cm^2. The effects of the driving voltage and driving frequency were studied, followed by the impact of the spacing between the heater and the orifice plate on the heat transfer coefficient. An orifice plate with an orifice diameter of 1.52 mm was chosen. The spacing between the heater and the orifice plate was initially set to 5 mm.

The experiments were conducted by setting the driving frequency and varying the driving voltage from 40 to 60 V in steps of 10 V. The driving frequency was varied between 200 and 350 Hz in steps of 25 Hz. Fig. 15 shows the frequency effect on the nondimensional excess wall temperature for all three voltages, reflecting a parabolic dependence of the heat transfer coefficient on frequency, reaching a maximum value in the frequency range of 275–300 Hz.

To further explore the variation of enhancement with driving voltage, the driving frequency was set at 275 Hz, the observed optimum frequency, and the driving voltage varied from 40 to 120 V in steps of 10 V. It was concluded that the improvement ratio increased monotonically with the driving voltage in the range of driving voltages studied [83]. Use of the synthetic jet showed a 3.8 fold enhancement in natural convection at the optimum frequency for the peak driving voltage studied.

B. Pool Boiling

The results for the synthetic jet enhancement of boiling heat transfer at a bulk temperature of 30 °C are presented in Fig. 16. It may be seen that significant boiling enhancement was obtained in the low heat flux range studied. The most significant heat flux enhancement, by nearly a factor of four, was observed at low surface superheat, due, perhaps, to an earlier boiling incipience with the synthetic jet. The enhancement was found to diminish

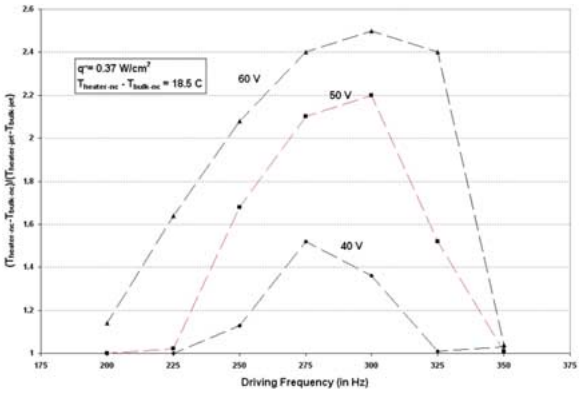

Fig. 15. *Effect of driving frequency on synthetic jet heat transfer in natural convection [81].*

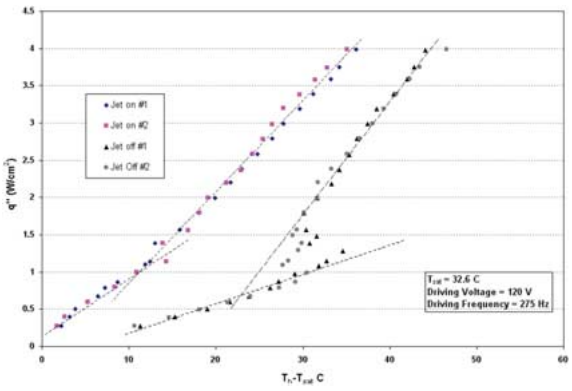

Fig. 16. *Synthetic jet enhancement of boiling heat transfer 30 °C [81].*

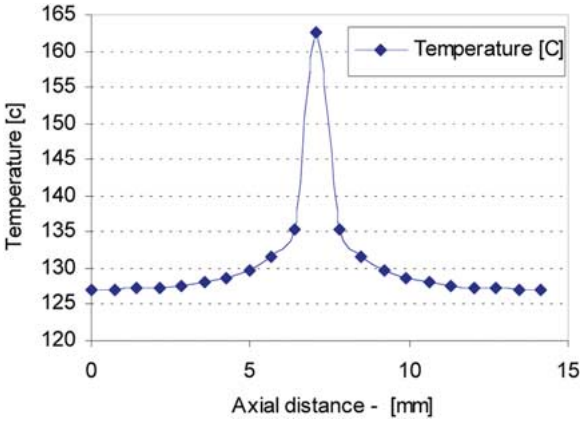

Fig. 18. *Temperature distribution across diagonal of chip [q_{chip} = 100 W/cm^2, q_{spot} = 2000 W/cm^2, h = 10 000 W/m^2–k, Tc = 22 °C].*

as the heat flux increased into the range of fully developed nucleate boiling [81].

X. HOT-SPOT THERMAL MANAGEMENT WITH DIRECT LIQUID COOLING

To assess the efficacy of direct liquid cooling for thermal management of high heat dissipation chips with concentrated high heat flux "hot spots," it is instructive to simulate the thermal performance of a notional advanced semiconductor chip cooled by the direct liquid cooling techniques discussed in previous sections. A 10 × 10-mm silicon chip, 0.5-mm (500 μm) thick, dissipating a uniform heat flux of 100 W/cm^2 across nearly all the active chip area serves as the test vehicle for this simulation. The chip is assumed to possess a central circular hot spot, varying from 100 to 400 μm in diameter and dissipating between 1 and 2 kW/cm^2. It is further assumed that the thermal conductivity of the silicon chip is invariant at 125 W/mK and that it is cooled from the back surface (opposite to that of the active circuitry) with heat transfer coefficients that can vary from 5 to 20 kW/m^{2}k, reflective of the values that can be achieved with the direct dielectric liquid cooling techniques described in previous sections and that the liquid temperature is 22 °C.

Fig. 17 presents the 3-D temperature profile, while Fig. 18 depicts the temperature along a diagonal on the active face of the silicon chip for a baseline directly cooled chip configuration with a 400-μm hot spot, generating a 2-kW/cm^2 heat flux, with the entire chip cooled from the back by a heat transfer coefficient of 10 kW/m^{2}k. As it can be seen from Figs. 17 and 18, when this notional baseline chip with a very severe "hot spot" is cooled by an FC liquid at 22 °C with an h equal to 10 kW/m^{2}k, it experiences an elevated average temperature of approximately 130 °C and a significant hot spot with a maximum temperature of 163 °C, or some 33 °C above the average chip temperature. The average and peak temperatures for various other combinations of the specified parameters are shown in Tables 2 and 3.

Tables 2 and 3 present the results for a hot spot diameter of 100 and 400 μm, respectively, with various hot spot heat fluxes and a range of heat transfer coefficients associated with the different direct liquid cooling techniques. In these tables, the first and second columns present

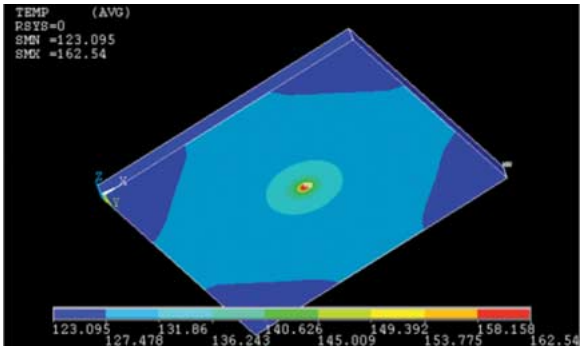

Fig. 17. *Three-dimensional temperature profile for direct liquid cooling of advanced semiconductor chip [10 × 10 × 0.5 mm, q'' = 100 W/cm^2, q''_{hs} = 2 kW/cm^2, d_{hs} = 400 μm, h = 10 W/m^2–k].*

Table 2 Temperatures for 100-μm Hot Spot Diameter for Various Heat Flux and Cooling Conditions

q_{spot} [W/cm^2]	h [W/m^{2}K]	T_{chip} [°C]	T_{conv} [°C]	T_{spot} [°C]	T_{spot_max} [°C]
1000	20000	76.2	74.2	78.9	79.7
1000	10000	126.2	124.2	129.0	129.7
1000	5000	226.3	224.3	229.1	229.8
2000	20000	76.4	74.4	82.2	83.8
2000	10000	126.5	124.6	132.3	134.0
2000	5000	226.7	224.7	232.5	234.1

Table 3 Temperatures for 400-μm Hot Spot Diameter for Various Heat Flux and Cooling Conditions

q_{spot} [W/cm^2]	h [W/m^{2}K]	T_{chip} [°C]	T_{conv} [°C]	T_{spot} [°C]	T_{spot_max} [°C]
1000	20000	77.5	75.6	89.1	92.2
1000	10000	128.2	126.4	140.2	143.3
1000	5000	229.4	227.6	241.6	244.7
2000	20000	79.2	77.5	103.7	110.3
2000	10000	130.7	129.0	155.9	162.5
2000	5000	233.2	231.6	259.0	265.6

the hot spot flux and convective coefficients, respectively, while the next three columns provide the average temperature on the active side of the chip, the average temperature on the cooled (back) side of the chip, and the average hot spot temperatures. The last column in Tables 2 and 3 presents the maximum temperature on the active side of the silicon chip. Not surprisingly, the average chip temperature (on both the active and wetted surfaces) is seen to vary directly with the convective/boiling heat transfer coefficient, while the on-chip hot spot temperature rise is conduction limited and—for the fixed chip geometry and thermal conductivity—is driven by the heat flux and size of the hot spot. Thus, as seen in Table 3, while raising the heat transfer coefficient to 20 kW/m^2k lowers the average chip temperature to 77 °C for a chip heat flux of 100 W/cm^2 and a liquid at 22 °C, the on-chip temperature rise for a 1-kW/cm^2 0.4-mm hot spot remains at approximately 15 K across the range of heat transfer coefficients from 5 kW to 20 kW/cm^2k. However, since the peak chip temperature is established by the super position of these two effects, any reduction in the average chip temperature has a salutary effect on the peak chip temperature, as well.

Thus, as also revealed in Fig. 19, direct liquid cooling, along with effective thermal spreading in the chip, appears to offer the potential for successfully limiting the chip and hot spot temperature rise to acceptable levels for a wide range of operating conditions. Most significantly, a heat transfer coefficient of 20 kW/m^2k could be used to effectively cool a 2-kW/cm^2 0.4-mm hot spot, along with maintaining an acceptable average temperature, for a 100-W/cm^2 chip.

Interestingly, the on-chip temperature rise—of the hot spot center relative to the chip average—can be seen to vary almost directly with the product of the heat flux and diameter, yielding a nine-fold increase from 3.6 K for a 0.1-mm 1-kW/cm^2 hot spot to 32.4 K for a 0.4-mm 2-kW/cm^2 hot spot. Due to the superposition of the convective and conductive effects, it may also be noted that while a large change (approximately 50%) in the maximum excess temperature results from increasing the flourinert heat transfer coefficient from 5 to 10 kW/m$^2 - k$, further increases to 20 kW/m$^2 - k$ only reduces the maximum temperature rise by approximately 30%.

XI. CLOSURE

The preceding has provided a comprehensive review of direct dielectric liquid cooling techniques that hold promise for addressing the on-chip hotspots encountered on advanced semiconductor chips now nearing commercialization. Published results and the available correlations for the heat transfer coefficients, and the CHF/dryout limits associated with pool boiling, gas-assisted evaporative cooling, single/multiple-jet impingement, spray cooling, and synthetic jet cooling have been presented and discussed.

Passive immersion cooling, relying on subcooled pool boiling, offers distinct advantages for thermal management of advanced microprocessor chips. Without the investment of pumping power and with no moving parts, use of mixtures of the Novec fluids, along with microporous surface coatings, subcooling, and elevated pressure, appears capable of removing as much as 100 W/cm^2 from a chip and limits the temperature rise on a large range of anticipated hot spots.

The high velocity flow of a liquid–gas mixture in the narrow channels between populated substrates offers the possibility of increasing the peak heat flux, as well as the volumetric thermal management capability of direct liquid cooling, at the expense of considerable pumping power, meso-scale plumbing, and controls, and requires some effort to separate the inert gas from the generated vapor. While promising results have been achieved with this technique, much additional effort will be required to develop the theoretical, as well as empirical, relations needed to design and optimize such gas-assisted evaporative cooling systems for a wide range of high heat flux applications. The high convective heat transfer coefficients that can be attained by submerged and free-surface

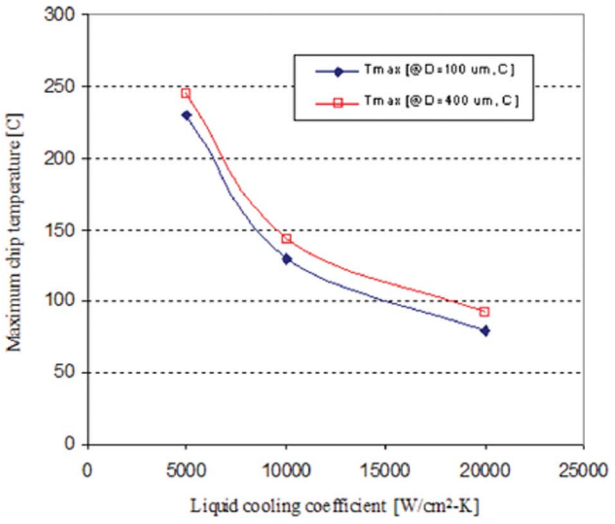

Fig. 19. *Effect of convective coefficient on hot spot temperature for* $qhs'' = 1000$ W/cm^2.

impinging jets, along with the ability to vary and control the heat transfer rate across a large surface with an appropriately configured liquid distribution plate, have made jet impingement one of the most promising alternatives in direct liquid cooling of electronic components. Despite the complex behavior of the local heat transfer coefficient resulting from parametric variations in the impinging jet flow, it has been found possible to correlate the average heat transfer coefficient with a single, relatively simple, expression, for both individual jets and arrays of jets and to thus provide the designer with the tools needed to tailor the jet array design to the thermo fluid needs of specific applications.

While it is generally agreed that spray and jet impingement provide similar heat transfer coefficient and critical heat flux values, for similar pumping power, volume, and cost, liquid spray appears to result in a more uniform temperature profile on the heater surface and to be less susceptible to disruption by vigorous boiling in the impingement zone. However, the application of spray cooling is presently limited by concerns relative to the durability of spray nozzles, including inconsistent spray characteristics, erosion, and clogging due to the very small orifice diameter and high pressure required to produce the desired droplet diameters. Moreover, the relative contributions of the various phenomena involved in spray cooling have so far eluded detailed characterization.

Meso-scale microfluidic devices, notably pumps, valves, and switches, capable of enhancing single or two phase flow, as well as spray cooling, continue to attract considerable interest for direct liquid cooling of electronics components. While use of liquid synthetic jets has shown significant enhancement in both natural convection and low heat flux pool boiling, it appears that further advances in understanding and implementation will be needed to implement synthetic jets in high flux electronic cooling applications.

Although successful commercialization of advanced passive, as well as active, phase-change cooling requires considerable exploratory phenomenological research, experimental determination of limits and transfer rates, and development of reliable low-cost hardware, the foregoing has revealed that direct dielectric liquid cooling can provide a most promising set of alternatives for the thermal management of next generation microprocessor chips, even in the presence of severe hot spots. Application of the very high heat transfer coefficients associated with enhanced pool boiling, jet impingement, spray cooling, and gas-assisted flow boiling directly to the back surface of the chip appears to offer the potential for successfully limiting the chip and hot spot temperature rise to acceptable levels for a wide range of operating conditions. ■

Acknowledgment

The authors would like to thank Dr. J. Qi, formerly of the University of Maryland, and Dr. A. Watwe, Intel Corporation, for their help in defining the scope and identifying the literature to be explored in the preparation of this manuscript.

REFERENCES

[1] iNEMI. (2004). Electronics Manufacturing Initiative Technology Roadmap. [Online]. Available: http://www.nemi.org

[2] A. Watwe and R. Viswanath, "Thermal implications of non-uniform die power map and CPU performance," presented at the Inter PACK'03, Maui, HI.

[3] 3M Specialty Fluids. (2006). [Online]. Available: http://www.3m.com/market/industrial/fluids/library

[4] A. D. Kraus and A. Bar-Cohen, *Thermal Analysis and Control of Electronic Equipment*. New York: McGraw-Hill, 1982.

[5] A. Bar-Cohen and T. W. Simon, "Wall superheat excursions in the boiling incipience of dielectric fluids," *Heat Transf. Eng.*, vol. 9, no. 3, pp. 19–31, 1988.

[6] A. Bar-Cohen, "Thermal management of air- and liquid-cooled multichip modules," *IEEE Trans. Compon., Hybrids, Manuf. Technol.*, vol. CHMT-10, no. 2, pp. 159–175, Jun. 1987.

[7] D. Tuckerman and F. Pease, "High performance heat sinking for VLSI," *IEEE Electron Device Lett.*, vol. EDL-2, no. 5, pp. 126–129, May 1981.

[8] S. Oktay and H. C. Kammerer, "A conduction cooled module for high performance LSI devices," *IBM J. Res. Dev*, vol. 26, no. 1, pp. 55–56, 1982.

[9] A. E. Bergles and A. Bar-Cohen, "Direct liquid cooling of microelectronic components," in *Advances in Thermal Modeling of Electronic Components and Systems*. New York: ASME, 1990, vol. 2, pp. 233–342.

[10] R. D. Danielson, Tousignant, and A. Bar-Cohen, "Saturated pool boiling characteristicsof commercially available perflourinated liquids," *Proc. ASME/JSME Thermal Engineering Joint Conf.*, vol. 3, pp. 419–430, 1987.

[11] G. Sherwood and S. Cray, Gas–liquidforced turbulence cooling, U.S. Patent 5 131 233, 1992.

[12] A. Vacca, D. Resnick, D. Frankel, R. Back, J. Kreilich, and D. Carlson, "A cryogenically-cooled CMOSVLSI super-computer," *VLSI Syst. Des.*, vol. 8, pp. 80–88, 1987.

[13] P. Ing, C. Sperry, R. Philstrom, P. Claybaker, J. Webster, and R. Cree, "Supercomputer cooling system," in *Proc. 43rd Electronic Components Technology Conf.*, 1993, pp. 218–237.

[14] A. O. Greene and J. C. Wightman, Cooling electronic equipment by direct evaporation of liquid refrigerant, Wright-Patterson AFB, OH, Air Material Command Rep. PB 136065, 1948.

[15] M. Mark, M. Stephenson, and C. E. Goltsos, "An evaporative-gravity technique for airborne equipment cooling," *Trans. IRE*, vol. ANE-5, pp. 47–52, Mar. 1958.

[16] D. L. Cochran, "Boiling heat transfer in electronics," *Electron. Packag. Prod.*, vol. 8, no. 7, pp. CL3–CL7, 1968.

[17] G. Pautsch and A. Bar-Cohen, "Thermal management of multichip modules with evaporative spray cooling," in *Advances in Electronic Packaging, Proc. InterPack*, 1999, pp. 1453–1463.

[18] S. M. You, T. W. Simon, and A. Bar-Cohen, "Experimental investigation of nucleate boiling incipience with highly wetting dielectric fluid (R113)," *Int. J. Heat Mass Transf.*, vol. 33, no. 1, pp. 105–118, 1990.

[19] W. M. Rohsenow, "A method of correlating heat transfer data for surface boiling of liquids," *Trans. ASME*, Jul. 1952.

[20] S. S. Kutateladze, "A hydrodynamic theory of changes in the boiling process under free convection conditions," *Izv. Akad. Nauk SSSR, otd. Tekhn. Nauk*, no. 4, pp. 529, 1951, Translated in AEC-TR-1441.

[21] N. Zuber, Atomic Energy Commission Rep. AECU-4439, Atomic energy commission technical information service, 1959.

[22] R. F. Gaertner and J. W. Westwater, "Population of active sites in nucleate boiling heat transfer," in *Chem. Eng. Prog. Symp. Ser.*, 1960, pp. 39–48.

[23] R. F. Gaertner, "Photographic study of nucleate pool boiling on a horizontal surface," *ASME J. Heat Transf.*, vol. 87, pp. 17–29, 1965.

[24] Y. Haramura and Y. Katto, "A new hydrodynamic model of critical heat flux applicable widely to both pool and forced convective boiling on submerged bodies in saturated liquids," *Int. J. Heat Mass Transf.*, vol. 26, pp. 389–399, 1983.

[25] D. B. Kirby and J. W. Westwater, "Bubble and vapor behavior on a heated horizontal plate during pool boiling near burnout," in *Chem. Eng. Prog. Symp. Ser.*, 1965, pp. 238–248.

[26] H. J. Van Quwerkerk, "Burnout in pool boiling—The stability of boiling mechanisms," *Int. J. Heat Mass Transf.*, vol. 15, pp. 25–34, Jan. 1972.

[27] J. M. Ramilson and J. H. Lienhard, "Transition boiling heat transfer and film transition regime," *J. Heat Transf.*, vol. 109, pp. 746–752, 1987.

[28] T. G. Theofanous, J. P. Tu, A. T. Dinh, and T. N. Dinh, "The boiling crisis phenomenon—Part I: Nucleation and nucleate boiling heat transfer," *Exp. Thermal Fluid Sci.*, vol. 26, no. 6, pp. 775–792, Aug. 2002.

[29] A. Bar-Cohen, A. Watwe, and M. Arik, "Pool boiling critical heat flux in dielectric liquids," presented at the 5th Int. Conf. Boiling Heat Transfer, Montego Bay, Jamaica, 2003.

[30] A. Watwe, A. Bar-Cohen, and A. McNeil, "Combined pressure and subcooling effects on pool boiling from a PPGA chip package," *J. Electron. Packag.*, vol. 199, pp. 95–105, Jun. 1997.

[31] A. A. Watwe and A. Bar-Cohen, "Modeling conduction effects on pool boiling critical heat flux of dielectric liquids," in *Proc. Nat. Heat Transfer Conf.*, 1997, pp. 35–43.

[32] M. Arik and A. Bar-Cohen, "Effusivity-based correlation of surface property effects in pool boiling CHF of dielectric liquids," *Int. J. Heat Mass Transf.*, vol. 46, pp. 3755–3765, 2003.

[33] ——, "Ebullient cooling of integrated circuits by Novec fluids," presented at the ASME/ IEEE Pacific Rim/Int., Intersociety, Electronic Packaging Technical/Business Conf. Exhibition, Kauai, HI, 2001, ASME Paper 15515.

[34] A. A. Watwe and A. Bar-Cohen, "Enhancement of the pool boiling CHF using dielectric liquid mixtures," presented at the Engineering Foundation Conf., Convective Flow Pool Boiling, Irsee, Germany, 1997.

[35] M. Arik, "Enhancement of pool boiling critical heat flux in dielectric liquids," Ph.D. dissertation, Dept. Mechanical Eng., Univ. Minnesota, Minneapolis, 2001.

[36] S. Ahmed and V. P. Carey, "Effects of gravity on the boiling of binary fluid mixtures," *Int. J. Heat Mass Transf.*, vol. 41, no. 16, pp. 2469–2483, 1998.

[37] A. Bar-Cohen, G. Sherwood, M. Hodes, and G. Solbreken, "Gas-assisted evaporative cooling of high density electronic modules," *IEEE Trans. Compon., Packag., Manuf. Technol. A*, vol. 18, no. 3, pp. 502–509, Sep. 1995.

[38] K. Jambunathan, E. Lai, M. A. Moss, and B. L. Button, "A review of heat transfer data for single circular jet impingement," *Int. J. Heat Fluid Flow*, vol. 13, pp. 106–115, 1992.

[39] B. W. Webb and C. F. Ma, "Single phase liquid jet impingement heat transfer," *Adv. Heat Transf.*, vol. 26, pp. 105–217, 1995.

[40] H. Wolf, F. P. Incropera, and R. Viskanta, "Jet impingement boiling," *Adv. Heat Transf.*, vol. 23, pp. 1–132, 1992.

[41] X. S. Wang, Z. Dagan, and M. L. JiJi, "Heat transfer between a circular free impinging jet and a solid surface with non-uniform wall temperature or wall heat-flux-2: Solution for the boundary layer region," *Int. J. Heat Mass Transf.*, vol. 32, no. 7, pp. 1361–1371, 1989.

[42] X. Liu, J. H. Lienhard, and J. S. Lombara, "Convective heat transfer by impingement of circular liquid jets," *ASME J. Heat Transf.*, vol. 113, pp. 571–581, 1991.

[43] C. F. Ma, Y. H. Zhao, T. Masuoka, and T. Gomi, "Analytical study on impingement heat transfer with single-phase free-surface circular liquid jets," *J. Thermal Sci.*, vol. 5, no. 4, pp. 271–277, 1996.

[44] D. M. Schafer, S. Ramadhyani, and F. P. Incropera, "Numerical simulation of laminar convection heat transfer from an in-line array of discrete sources to a confined rectangular jet," *Numer. Heat Transf. A*, vol. 22, pp. 121–141, 1992.

[45] M. M. Rahman and A. J. Bula, "Numerical modeling of conjugate heat transfer during free liquid jet impingement," in *Proc. ASME Advanced Energy Systems Division*, 1998, pp. 475–486.

[46] H. Fujimoto, T. Hirohiko, N. Hatta, and R. Viskanta, "Numerical simulation of transient cooling of a hot solid by an impinging free surface jet," *Numer. Heat Transf. A*, vol. 36, pp. 767–780, 1999.

[47] D. J. Womac, F. P. Incropera, and S. Ramadhyani, "Correlating equations for impingement cooling of small heat sources with multiple circular liquid jets," *ASME J. Heat Transf.*, vol. 116, pp. 482–486, 1994.

[48] H. Sun, C. F. Ma, and Y. C. Chen, "Prandtl number dependence of impingement heat transfer with circular free-surface liquid jets," *Int. J. Heat Mass Transf.*, vol. 14, no. 10, pp. 1360–1363, 1998.

[49] H. Martin, "Heat and mass transfer between impinging gas jets and solid surfaces," *Adv. Heat Transf.*, vol. 8, pp. 1–60, 1977.

[50] K. A. Estes and I. Mudawar, "Comparison of two-phase electronic cooling using free jets and sprays," *ASME J. Electron. Packag.*, vol. 117, pp. 323–332, 1995.

[51] C. F. Ma and A. E. Bergles, "Boiling jet impingement cooling of simulated microelectronic chip," in *Proc. ASME 1983 Winter Annu. Meeting*, pp. 5–12.

[52] ——, "Jet impingement nucleate boiling," *Int. J. Heat Mass Transf.*, vol. 29, pp. 1095–1101, 1986.

[53] T. Nonn, Z. Dagan, and L. M. Jiji, "Jet impingement flow boiling of a mixture of FC-72 and FC-87 liquids on a simulated electronic chip," *Heat Transf. Electron.*, vol. 111, pp. 121–128, 1989.

[54] D. C. Wadsworth and I. Mudawar, "Cooling of a multichip electronic module by means of confined two-dimensional jets of dielectric liquid," *ASME J. Heat Transf.*, vol. 112, pp. 891–898, 1990.

[55] ——, "Enhancement of single-phase heat transfer and critical heat flux from an ultra-high-flux simulated microelectronic heat source to a rectangular impinging jet of dielectric liquid," *ASME J. Heat Transf.*, vol. 114, pp. 764–768, 1992.

[56] G. M. Chrysler, R. C. Chu, and R. E. Simons, "Jet impingement boiling of a dielectric coolant in narrow gaps," in *Proc. IEEE Intersoc. Conf. Thermal Phenomena*, 1994, pp. 1–8.

[57] D. Copeland, "Single-phase and boiling cooling of a small heat source by multiple nozzle jet impingement," *Int. J. Heat Mass Transf.*, vol. 39, no. 7, pp. 1395–1406, 1998.

[58] W. Nakayama and D. Copeland, "Heat transfer from chips to dielectric coolant: Enhanced pool boiling versus jet impingement cooling," *Enhanced Heat Transf.*, vol. 1, no. 3, pp. 231–243, 1994.

[59] I. Mudawar and D. C. Wadsworth, "Critical heat flux from a simulated electronic chip to a confined rectangular impinging jet of dielectric liquid," *Int. J. Heat Mass Transf.*, vol. 34, pp. 1465–1480, 1991.

[60] S. V. Garimella and R. A. Rice, "Heat transfer in submerged and confined liquid jet impingement," *Heat Transf. High Heat Flux Syst.*, vol. 301, pp. 59–68, 1994.

[61] ——, "Confined and submerged liquid jet impingement heat transfer," *ASME J. Heat Transf.*, vol. 117, pp. 871–877, 1995.

[62] H. Sun, C. F. Ma, and W. Nakayama, "Local characteristics of convective heat transfer from simulated microelectronic chips to impinging submerged round water jets," *ASME J. Electron. Packag.*, vol. 115, pp. 71–77, 1993.

[63] D. E. Maddox and A. Bar-Cohen, "Thermofluid design of single phase submerged-jet impingement cooling for electronic components," *ASME J. Electron. Packag.*, vol. 116, pp. 237–240, 1994.

[64] M. Monde, "Critical heat flux in saturated forced convective boiling on a heated disk with an impinging jet," *Wäerme-und Stroffüebertrag*, vol. 19, pp. 205–209, 1985.

[65] T. Nonn, Z. Dagan, and L. M. Jiji, "Boiling jet impingement cooling of simulated microelectronic heat sources," ASME Paper WA/EEP-3, 1988.

[66] Z. H. Liu and Q. Z. Zhu, "Predication of critical heat flux for convective boiling of saturated water jet impingement on the stagnation zone," *ASME J. Heat Transf.*, vol. 124, pp. 1125–1130, 2002.

[67] Z. H. Liu, T. F. Tong, and Y. H. Qiu, "Critical heat flux of steady boiling for subcooled water jet impingement on the flat stagnation zone," *ASME Trans. J. Heat Transf.*, vol. 126, pp. 179–183, 2004.

[68] D. J. Womac, F. P. Incropera, and S. Ramadhyani, "Correlating equations for impingement cooling of small heatsources with multiple circular liquid jets," *ASME J. Heat Transf.*, vol. 116, pp. 482–486, 1994.

[69] S. C. Yao, S. Deb, and N. Hammouda, "Impact spray boiling for thermal control of electronic systems," *Heat Transf. Electron.*, vol. 111, pp. 129–133, 1989.

[70] C. F. Ma, Y. Q. Tien, H. Sun, D. H. Lei, and A. E. Bergles, "Local characteristics of heat transfer from vertical small heater to impinging round jet of liquid of larger Pr number," in *Heat Transfer Enhancement and Energy Conservation*, S. J. Deng, Ed. Bristol, PA: Hemisphere, 1990, pp. 223–229.

[71] M. R. Pais, L. C. Chow, and E. T. Mahefkey, "Surface roughness and its effects on the heat transfer mechanism in spray cooling," *J. Heat Transf.*, vol. 114, pp. 211–219, 1992.

[72] S. Chandra and C. T. Avedisian, "On the collision of a droplet with a solid surface," *Proc. R. Soc. Lond.*, vol. 432, pp. 13–41, 1991.

[73] S. Inada, Y. Miyasaka, K. Sakamoto, and K. Hojo, "Liquid-solid contact state and fluctuation of the vapor film thickness of a drop impinging on a heated surface," *J. Chem. Eng. Jpn.*, vol. 21, pp. 463–468, 1988.

[74] F. K. McGinnis and J. P. Holman, "Individual droplet heat transfer rates for splattering on hot surfaces," *Int. J. Heat Mass Transf.*, vol. 12, p. 95, 1969.

[75] K. A. Estes and I. Mudawar, "Correlating of Sauter mean diameter and critical heat flux for spray cooling of small surface," *Int. J. Heat Mass Transf.*, vol. 38, pp. 2985–2996, 1995.

[76] M. S. Sehmbey, L. C. Chow, O. J. Hahn, and M. R. Pais, "Effect of spray characteristics on spray cooling with liquid nitrogen,"

J. Thermophys. Heat Transf., vol. 9, no. 4, pp. 757–765, 1995.

[77] C. Cho and R. Ponzel, "Experimental study on the spray cooling of a heated solid surface," in *Proc. ASME Fluids Eng. Div.*, 1997, pp. 265–272.

[78] S. Jiang and V. K. Dhir, "Spray cooling in a closed system with different fractions of non-condensibles in the environment," *Int. J. Heat Mass Transf.*, vol. 47, pp. 5391–5406, 2004.

[79] A. L. Minichiello, J. G. Hartley, A. Glezer, and W. Z. Black, "Thermal management of sealed electronic enclosures using synthetic jet technology," in *Advances in Electronic Packaging, Proc. InterPack*, 1997, pp. 1809–1812.

[80] J. Garg, M. Arik, S. Weaver, T. Wetzel, and S. Saddoughi, "Advanced localized air cooling with synthetic jets," *ASME J. Electron. Packag.*, pp. 503–511, Dec. 2005.

[81] J. Garg, M. Arik, A. Bar-Cohen, R. Wolf, B. Vukasinovic, J. G. Hartley, and A. Glezer, "Synthetic jet enhancement of natural convection and pool boiling in a dielectric liquid," presented at the Int. Heat Transfer Conf., Paris, France, 2002.

ABOUT THE AUTHORS

Avram Bar-Cohen (Fellow, IEEE) is a Distinguished University Professor and Chair of the Mechanical Engineering Department, University of Maryland, College Park, where he continues his research in the thermal management of Micro/Nano systems. He is coauthor (with A. D. Kraus) of *Design and Analysis of Heat Sinks* (Wiley, 1995) and *Thermal Analysis and Control of Electronic Equipment* (Hemisphere, 1983) and has co-edited nine books in this field. He has authored and coauthored approximately 250 journal papers, refereed proceedings papers, and chapters in books and has delivered more than 50 keynote, plenary, and invited lectures at major technical conferences and institutions. He has advised to completion 52 Ph.D. and M.S. students.

Dr. Bar-Cohen currently serves as the Editor-in-Chief of the three IEEE CPMT Transactions, is on the Steering Committee of ASME's Nanotechnology Institute, and is the ASME representative for the United States on the Assembly for International Heat Transfer Conferences.

Mehmet Arik (Member, IEEE) was born in Turkey in 1969. He received the B.Sc. degree in mechanical engineering from Istanbul Technical University, Istanbul, Turkey, the M.Sc. degree from the University of Miami, Miami, FL, in 1996, and the Ph.D. degree from the University of Minnesota, Minneapolis, focusing on the thermal management of high flux electronic components and microelectromechanical systems, in 2001.

Since December 2000, he has worked as a Senior Thermal Scientist at the General Electric Global Research Center, Niskayuna, NY, on the thermal management of electronics. He has expertise in air-cooled and liquid-cooled power electronics, photonics packaging, and medical systems. He holds 11 U.S. patents and five are pending. He published over 30 papers in international journals and conferences in the fields of electronics cooling and MEMS.

Dr. Arik is a member of ASME and Sigma Xi.

Michael Ohadi is a Professor of mechanical engineering and the Acting Chief Academic Officer at the Petroleum Institute. An internationally recognized authority in enhanced heat and mass transfer in heat exchangers and energy systems, he has conducted many research projects for both industry and government and has published over 140 refereed technical papers

Dr. Ohadi is a Fellow of both ASME and ASHRAE and has won numerous awards from both societies.